IRANIAN JOURNAL OF PHYSICS RESEARCH

Iranian Journal of Physics Research, Vol. 8, No. 2, 2008

Many-body effects in low dimensional electron liquids

R Asgari

School of Physics, Institute for Studies in Theoretical Physics and Mathematics, 19395-5531 Tehran, Iran

(Received 5 December 2007)

Abstract

This review article is about the role of electron-electron interactions in low dimensional systems and its transport properties in nano-structures. It begins with a review of the pair-distribution function theory of electron liquid systems taking into account the electron-electron interactions. We extend the theory for highly correlated system such two- and one-dimensional electron liquids. We then review the microscopic theory of the local-field factors and calculate the quasiparticle properties in two-dimension electron liquid and compare our results with those measured by recent experiments. The physics of two-dimension bilayer structures are revised and are immediately applied to the study of charged Coulomb drag effects in a bilayer electron-electron system and results are compared with experimental data. As a final application, the Luttinger theory is discussed and we compare our recent calculations with those obtained from quantum Monte Carlo simulation for one dimensional electron liquid.

Keywords: electron liquid, electron-electron interactions, electron correlations, transport

1. Introduction

An interacting electron liquid (EL) on a uniform background with constant dielectric constant ε is used as the reference system in most realistic calculations of electronic structure in condensed matter physics [1]. Understanding the many body properties of this model has attracted continued interest for many decades. EL is usually defined by the only relevant parameter in the absence of magnetic field and spin-orbit interaction at zero temperature which is the Wigner-Seitz density parameter r_s defined by

$$r_s = \left(\frac{D}{n\Omega_D} \right)^{1/D} \frac{1}{a_B^*}, \qquad (1)$$

Were D is dimensionality, $\Omega_3 = 4\pi$, $\Omega_2 = 2\pi$ and considering $\Omega_1 = 2$, n is the electron density and $a_B^* = \varepsilon \mathrm{h}^2 / me^2$ is the effective Bohr radius. The behaviors of EL systems are not like classical systems. In the high density limit ($r_s \to 0$) associated with a large value of the kinetic energy, the EL behaves like a gas and electrons are highly itinerant. It means the typical time spent near a specific point is very short. In this case, the electron characteristic are well described by using a wave-like picture and physics of system is well explained by one-particle approximation. In the opposite limit, when r_s becomes large, electrons tend to see each other better and the effects of statistical correlations between the motions of individual electrons become important. In this case, electrons spend a large time around a lattice site (Wigner crystal [1]) and electrons behaves like a solid. Interestingly, a one-particle picture description would not be appropriate, specially at short or intermediate time scales. A particle like picture might in fact be more appropriate in large r_s than a wave like picture. In the intermediate density regime which is relevent in three dimensions for simple metals and in two dimensions for systems like the electrons in an inversion layer of a Si metal-oxide-semiconductor field-effect transistor (MOSFET) or in a GaAs quantum well in most density regimes, the EL is in a liquid state with intermediate-to-strong electron-electron coupling and moreover there is a competition between the wave like picture of electron and particle like one and validity of all theory based on either one particle pictures or perturbation approximations are questionable.

In the summer school, I gave two separate topics on strongly correlated Fermion systems. Firstly was about the correlations in low dimensional electron liquids and then two lectures about the ultracold Fermion gases, Feshbach resonance and BEC-BCC cross-over. Since the first part of my lecture notes regarding to the electron liquids is already long enough, I do not present any explanation about the ultarcold Fermi gases here and wish to write a brief review about this fascinating novel

subject in coming future. I would like to refer the reader to recent wonderful review by Giorgini, *et al.*[2] in the context of ultacold Fermi gases.

The rest of this lecture notes is organized as follows. In Sec. II, we introduce the theoretical approach for electron liquid system incorporating the many-body effects. We then extend the approach to two-dimensional system and try to revise the quasi properties of the system and compare our results with those measured recently with different experimental groups in section III. Section IV contains our numerical calculations of drag resistivity and comparison of models with experimental data. Section V we review the physics of non-Fermi liquid dealing with one-dimensional electron liquids and compare our results with those calculated within the sate-of-the-art Quantum Monte Carlo simulations. We conclude in Sec. VI with a brief summary.

2. Theoretical approach

In this section, we briefly describe the main theoretical generalities on homogenous quantum electron liquids. To this purpose, we start with noninteracting Fermi liquids and give some basic definitions and properties. After that by taking the Pauli exclusion principle into account, we describe the system with more physical important properties and then explain briefly all theoretical weakness in the strongly correlated regions. Finally we introduce our recent approach to explore correlated systems by incorporating better effective electron-electron interactions.

2.1. Ideal fermi gas and normal Fermi liquids

Let us start with a brief review of the microscopic states of an ideal Fermi gas. We consider a non-relativistic gas of N noninteracting fermions inside a dimensional (D) volume V, in the thermodynamic limit $V \to \infty$ and $N \to \infty$, at given particle-number density, $n = N/V$ finite. The eigenstates of the system are antisymmetric under the exchange of particles and are written as Slater determinants built from single-particle states $u_{k\sigma}(r)$. These are the product of (a) a plane wave $V^{-1/2}\exp(ik\cdot r)$ with wave vector k, momentum $\hbar k$ and energy $e_k = \hbar^2 k^2/(2m)$, and (b) a spin function. In particular the ground state is built from the plane waves of lowest energy, corresponding to values of $|\vec{k}|$ up to the *Fermi wave number* k_F. For spin-$1/2$ fermions in the paramagnetic state (equal numbers of up and down spins), k_F is determined by

$$N = \sum_{k,\sigma(k\le k_F)} 1 = 2\frac{V}{(2\pi)^d}\int_{(k\le k_F)} d^d k = 2\frac{V}{(2\pi)^d}\frac{\Omega_d}{d}k_F^d, \tag{2}$$

i.e. $k_F = (3\pi^2 n)^{1/3}$ for 3D. The plane waves entering the ground-state determinant fill a sphere of radius k_F in k space (the *Fermi sphere*). The momentum distribution $n(k)$ is the *average* occupation number of each single-particle state and in the ground state of the ideal Fermi gas jumps discontinuously from 1 to 0 as k crosses the surface of the Fermi sphere.

The excited states of the ideal Fermi gas are obtained by exciting particles from states inside the Fermi sphere to states outside it: that is, the elementary excitation process is the creation of a particle-hole pair. The particle and the hole are not correlated in the absence of interactions and we may also take a grand-canonical viewpoint: the elementary excitations of the gas are of two independent types, namely a particle added in a state outside the Fermi sphere (with $|\vec{k}| \ge k_F$ and energy e_k - μ, μ being the chemical potential) and a hole added in a state inside the Fermi sphere (with $|\vec{k}| \le k_F$ and excitation energy μ - e_k).

The homogeneous fluids of interacting fermions with physical interest in condensed matter physics are (1) liquid ^3He and (2) the sea of electronic carriers in a metal or a doped semiconductor. The ideal Fermi gas provides a good starting point for these systems in the normal state.

However, the interactions may lead to instabilities of the Fermi gas against a transition to (a) a superfluid state, which appears through the opening of a forbidden-energy gap between the ground state and the excited states; or to (b) a (partially or fully) magnetically ordered state, in which an energy gap is present for spin-flip processes at constant momentum. Moreover, for conduction electrons in reduced dimensionalities (D=1 and also in some 2D tight-binding-like models) a Luttinger liquid state may be induced by the electron-electron interactions. A Luttinger liquid differs from a normal Fermi liquid in two respects, *i.e.* (a) the discontinuity in the momentum distribution across the Fermi surface is replaced by another type of non-analytic behavior, and (b) spin-charge separation occurs [3].

2.2. Hartree-Fock theory of the degenerate electron liquid

The Hartree-Fock approximation [4] for the ground state of a system of interacting fermions assumes that the many-body wave function is a Slater determinant built from single-particle orbitals, to be determined self-consistently by minimization of the expectation value of the Hamiltonian. Whereas for an inhomogeneous many-electron system (*e.g.* an atom or a molecule) the solution of the Hartree-Fock self-consistent problem may usually be obtained only in a numerical form involving further approximations, the exact Hartree-Fock solution is immediately found in the case of a homogeneous fluid ($V_{ext}(r) = 0$): the self-consistent single-particle orbitals are necessarily plane waves, from the translational invariance of the system. Hence, the Hartree-Fock wave function for the ground state of a homogeneous fluid is the same as that of the ideal Fermi gas: that is, the

evaluation of the ground-state energy in Hartree-Fock is equivalent in this case to first-order perturbation theory.

Including explicitly the spin indices, we get

$$E_g^{HF} = \sum_{k,\sigma} e_k n^0_{k,\sigma} + \frac{1}{2}\sum_q v_q \sum_{k,\sigma}\sum_{k',\sigma'} \langle 0 \,|\, \hat{c}^\dagger_{k+q\sigma}\hat{c}^\dagger_{k'-q\sigma'}\hat{c}_{k'\sigma'}\hat{c}_{k\sigma} \,|\, 0\rangle \quad (3)$$

where $n^0_{k,\sigma}$ is the ideal Fermi distribution and $|\,0\rangle$ is the ground state of the ideal Fermi gas. The matrix element in Eq. (3) has non-zero value in two cases: (1) $q = 0$, and (2) $k' - k = q$ with $\sigma = \sigma'$ (these are known as the Hartree term and the exchange or Fock term, respectively). The energy may be written in the form (with $v_0 = v_{q=0}$)

$$\begin{cases} E_g^{HF} = \sum_{k,\sigma} n^0_{k,\sigma}\left[e_k + \frac{1}{2}\Sigma_{HF}(k)\right] \\ \Sigma_{HF}(k) = v_0 - \frac{1}{N}\sum_q v_q n^0_{k+q,\sigma}. \end{cases} \quad (4)$$

We see that the energy of a fermion with momentum k becomes $e_{HF}(k) = e_k + \Sigma_{HF}(k)$ as a consequence of the interactions. $\Sigma_{HF}(k)$ is the Hartree-Fock *self-energy* of a fermion. Its two terms derive from the fact that the fermion (a) feels the space average of the interaction potential, and (b) is kept apart by the Pauli symmetry of the many-body wave function from fermions having spin parallel to its own, so that their mutual interaction is decreased.

We continue this calculation for a 3D electron plasma (with interaction potential $v_q = 4\pi e^2 / q^2$) neutralized by a background of positive charge (the background must be added to ensure overall charge neutrality and leads to $v_0 = 0$). We get

$$\begin{cases} \Sigma_{HF}(k) = -\frac{e^2 k_F}{\pi}\left[1 + \frac{k_F^2 - k^2}{2kk_F}\ln\left|\frac{k+k_F}{k-k_F}\right|\right] \\ \frac{E_g^{HF}}{N} = \left(\frac{3}{5\alpha^2 r_s^2} - \frac{3}{2\pi\alpha r_s}\right) Ryd\,; \quad \left(\frac{2.21}{r_s^2} - \frac{0.916}{r_s}\right) Ryd. \end{cases} \quad (5)$$

Here $\alpha = (9\pi/4)^{-1/3}$ and r_s is defined by $4\pi(r_s a_B)^3/3 = 1/n$, with a_B being the Bohr radius [$k_F a_B = (\alpha r_s)^{-1}$]. As already remarked, the gain in potential energy found in Hartree-Fock derives from the fact that the exclusion principle keeps apart pairs of electrons with parallel spins, thus lowering on average their Coulomb repulsive interaction energy. Notice that the ratio between potential and kinetic energy is proportional to r_s: this dimensionless length gives a measure of the coupling strength, which increases *with decreasing density*.

The expression given above for $\Sigma_{HF}(k)$ predicts that the derivative of $e_{HF}(k)$ has a logarithmic divergence at $k = \pm k_F$: within Hartree-Fock the velocity of an electron on the Fermi surface (defined by $\hbar v_F = \nabla_k e_{HF}(k)\big|_{k=k_F}$) diverges and hence the effective mass m^* (defined by setting $v_F = \hbar k_F / m^*$) and the density of single-particle states (proportional to m^*) vanish on the Fermi surface. This result disagrees with experiment: *e.g.* it would give a $T/\ln T$ form for the dependence of the electronic heat capacity on temperature, instead of the linear T dependence which is observed in normal metals. The Landau theory of normal Fermi liquids restores the correct behavior. The main problem with the Hartree-Fock theory is that, by neglecting correlations due to Coulomb repulsions (which are most effective for electrons with antiparallel spins), it includes neither dielectric screening nor the collective plasma excitation.

All states of a spin-independent Hamiltonian are classified according to the eigenvalue S_z of the total spin along a chosen axis. The allowed values of S_z can range from 0 in the spin-compensated Fermi fluid so far considered up to $\pm N/2$ in the case when all spins point in the same direction. A partially spin-polarized state has $N_\uparrow$ spin-up and $N_\downarrow$ spin-down electrons, with $N_\uparrow + N_\downarrow = N$. The fractional spin polarization is $\zeta = (N_\uparrow - N_\downarrow)/N$, ranging from 0 to 1 (we are choosing $N_\uparrow$ as the number of majority spin).

For a Fermi gas with $\zeta \neq 0$ we need to define two distinct Fermi spheres with radii $k_{F\uparrow(\downarrow)} = k_F(1 \pm \zeta)^{1/3}$, leading to a free-particle kinetic energy given by

$$\frac{E_0(r_s,\zeta)}{N} = \frac{3}{10\alpha^2 r_s^2}\left[(1+\zeta)^{5/3} + (1-\zeta)^{5/3}\right] Ryd \quad (6)$$

in 3D. It is immediately seen from Eq. (6) that spin polarization increases the energy of the noninteracting Fermi gas, so that its ground state has $\zeta = 0$.

However, interactions may favor a ground state with a finite or full spin polarization for the phase diagram of the electron liquids. This is evident for the electron gas in the Hartree-Fock approximation. Each spin population independently contributes a term to the exchange energy, which is obtained using Eq. (5) as

$$\frac{E_x^{HF}(r_s,\zeta)}{N} = -\frac{3}{4\pi\alpha r_s}\left[(1+\zeta)^{4/3} + (1-\zeta)^{4/3}\right] Ryd. \quad (7)$$

In Hartree-Fock a fully ferromagnetic state ($\zeta = 1$) for the $3D$ electron gas becomes lower in energy than the paramagnetic state ($\zeta = 0$) at $r_s^{crit} = [2\pi(\sqrt[3]{4} - 1)]/[5\alpha(\sqrt[3]{2} - 1)]$; 5.45 .

2. 3. Lindhard susceptibility and RPA screening

The Random Phase approximation (RPA) first proposed by Bohm and Pines for the 3D EL replaces the proper

polarizability $\overset{\circ}{\chi}(\vec{q},\omega)$ by the density-density response function $\chi_0(\vec{q},\omega)$ of the ideal Fermi gas. Therefore, the plasma of interacting electrons is taken to respond as an ideal Fermi gas to the Hartree potential determined by the external charges and by the polarization charges, so that the electron-electron coupling is allowed only through the classical Coulomb interactions with the induced charges. The expression for the density response thus is

$$\chi^{RPA}(\vec{q},\omega) = \frac{\chi_0(\vec{q},\omega)}{1 - v_q \chi_0(\vec{q},\omega)}, \tag{8}$$

the numerator in this expression allows for the continuum of single electron-hole pair excitations, which is the only excitation mechanism for the ideal Fermi gas, whereas the denominator provides screening and is responsible for the resonance at the collective plasma mode. The plasmon sum rule and the perfect screening behavior are exactly satisfied, whereas the compressibility sum rule involves the ideal-gas compressibility.

The calculation of $\chi_0(\vec{q},\omega)$ in $3D$ was first tackled by Lindhard, in dealing with the scattering of a beam of fast electrons by excitation of density oscillations in the electronic structure of atoms in a gas. We proceed to calculate the inelastic scattering cross-section of an ideal Fermi gas, with the aim of using the Kramers-Kronig relations. The dynamic structure factor $S_0(q,\omega)$ (at energy transfer $\omega \geq 0$) is determined by the electron-hole pair excitations, *i.e.*

$$S_0(q,\omega) = \sum_{k,\sigma} n_k^0 (1 - n_{k+q}^0) \delta(\omega - e_{k+q} + e_k) \tag{9}$$

where $e_k = k^2/(2m)$ and $e_{k+q} - e_k = (k \cdot q + q^2/2)/m$ ($\hbar = 1$). $S_0(q,\omega)$ differs from zero only in the region of the (q,ω) plane enclosed by the curves $\omega_1(q) = (qk_F + q^2/2)/m$ and $\omega_2(q) = (-qk_F + q^2/2)/m$, thus, at given q one finds a continuum of excitations lying within this range of ω. In fact, (a) when the angle between k and q varies from 0 to π, the frequency spans the range $(-qk + q^2/2)/m \leq \omega \leq (qk + q^2/2)/m$; (b) on integration over k from 0 to k_F, the frequency spans the ranges $0 \leq \omega \leq \omega_1(q)$ for $q \leq 2k_F$ and $\omega_2(q) \leq \omega \leq \omega_1(q)$ for $q \geq 2k_F$. A full calculation of $S_0(q,\omega)$ yields

$$S_0(q,\omega) = \begin{cases} \pi\nu \dfrac{\omega}{qv_F} & for\ 0 \leq \omega \leq -\omega_2(q) \\ \pi\nu \dfrac{k_F}{2q} \left| 1 - \left(\dfrac{\omega}{qv_F} - \dfrac{q}{2k_F} \right)^2 \right| & for\ |\omega_2(q)| \leq \omega \leq \omega_1(q) \\ 0 & for\ \omega \geq \omega_1(q) \end{cases} \tag{10}$$

with $\nu = mk_F/(n\pi^2\hbar^2) =$ density of states for free electrons at the Fermi level and $v_F = \hbar k_F/m$. This result (multiplied by $-n/2$) yields $\Im m\chi_0(q,\omega)$ for $\omega > 0$; recalling that $\Im m\chi_0(q,\omega)$ is an odd function of ω and using the Kramers-Kronig relations one finds

$$\Re e\chi_0(q,\omega) = -n\nu \left\{ \frac{1}{2} + \frac{1}{8y}[1 - (x-y)^2] \ln \left| \frac{x-1-y}{x+1-y} \right| + \frac{1}{8y}[1 - (x+y)^2] \ln \left| \frac{x+1+y}{x-1+y} \right| \right\} \tag{11}$$

where $x = \omega/(qv_F)$ and $y = q/(2k_F)$.

The properties of 3D screening in the RPA are as follows.

(a) *Plasma excitation*. In the long-wavelength limit one gets $\Im m\chi_0(q,\omega) = 0$ and $_4$. The plasmon as obtained from the zero in the RPA dielectric function has frequency given by $\omega^2(q) = \omega_p^2 + 6\varepsilon_F q^2/(5m) + \ldots$ and is undamped with increasing q till the dispersion curve meets the electron-hole pair continuum (at $q = q_c$ say, with $q_c \approx k_F$). ``Landau damping" of the plasmon starts at q_c since the momentum and energy of the collective excitation may then be dissipated by the excitation of an electron-hole pair. However, one may show that in a more refined theory the damping of the plasmon should start already at terms of order q^2, through decay into *two* correlated electron-hole pairs.

(b) Static screening. We first present an alternative derivation of the static RPA dielectric function, which illustrates its physical content by working directly in space. The Hartree potential $V_H(r)$ created at a distance from a static foreign point charge of magnitude e should be evaluated self-consistently from the Poisson equation: $\nabla^2 V_H(r) = -4\pi e^2[\delta(r) + \delta n(r)]$, where $\delta n(r)$ is the induced change in electronic density. The electron density $n(r)$ may be written as $n(r) = 2\sum_k |\psi_k(r)|^2$, where $\psi_k(r)$ are single-electron orbitals, the sum over k is restricted to occupied orbitals ($|k| \leq k_F$) and the factor 2 comes from the sum over spin orientations. We must now calculate how the orbitals $\psi_k(r)$ in the presence of the foreign charge differ from plane waves $\exp(ik \cdot r)$: we use for this purpose the Schrödinger equation $\nabla^2\psi_k(r) + [k^2 - 2mV_H(r)/\hbar^2]\psi_k(r) = 0$, having imposed that the orbitals reduce to plane waves with energy $\hbar^2k^2/(2m)$ at large distance from the foreign charge. This approach (which will lead to the RPA result) is approximate insofar as the potential entering the Schrödinger equation has been taken as the Hartree potential, thus neglecting exchange and correlation

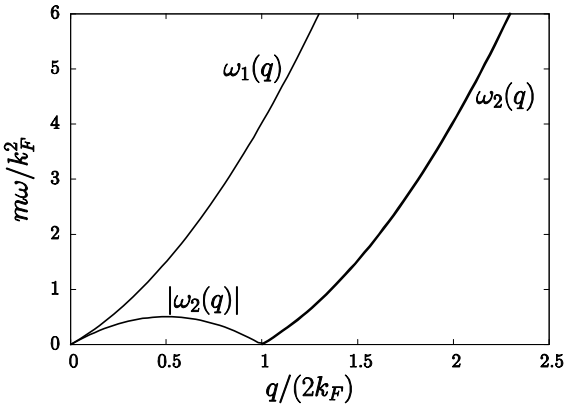

Figure 1. The continuum of electron-hole pair excitations in the 3D ideal Fermi gas. Adopted from Ref.[5] .

between an incoming electron and the screening cloud of the foreign charge.

With the aforementioned boundary condition the Schrödinger equation may be converted into an integral equation,

$$\psi_k(r) = \frac{1}{\sqrt{V}}\exp(ik\cdot r) + \frac{2m}{\hbar^2}\int d^3r' G_k(r-r')V_H(r')\psi_k(r') \tag{12}$$

with $G_k(r-r') = -\exp(ik\,|\,r-r'\,|)/(4\pi\,|\,r-r'\,|)$. The low-order perturbative solution (within linear response) is obtained upon replacing $\psi_k(r)$ by $V^{-1/2}\exp(ik\cdot r)$ inside the integral. This yields

$$\delta n(r) = -[mk_F^2/(2\pi^3\hbar^2)]\int d^3r'\, j_1(2k_F\,|\,r-r'\,|)\times [V_H(r')/\,|\,r-r'\,|^2]\ ,$$

where $j_1(x) = [\sin(x) - x\cos(x)]/x^2$ is a spherical Bessel function. Using this result in the Poisson equation and solving it by taking Fourier transform, we get $V_H(q) = 4\pi e^2/[q^2\varepsilon(q)]$ with

$$\varepsilon(q) = 1 + \frac{2mk_Fe^2}{\pi\hbar^2q^2}\left[1 + \frac{k_F}{q}\left(\frac{q^2}{4k_F^2} - 1\right)\ln\left|\frac{q-2k_F}{q+2k_F}\right|\right]. \tag{13}$$

This is the static dielectric function in RPA.

For $q \to 0$ this expression gives $\varepsilon(q) \to 1 + \kappa_{TF}^2/q^2$ with $\kappa_{TF}^2 = 3\omega_p^2/v_F^2$, *i.e.* the result of the Thomas-Fermi theory. However, $\varepsilon(q)$ has a singularity at $q = \pm 2k_F$, where its derivative diverges logarithmically: the discontinuity in the momentum distribution across the Fermi surface introduces a singularity in elastic scattering processes with momentum transfer equal to $\pm 2k_F$. This singularity determines after Fourier transform the behavior of $V_H(r)$ at large : $V_H(r)$ is an oscillating function rather than a monotonically decreasing function as in the Thomas-Fermi theory [6]. Indeed,

$$V_H(r) = \int\frac{d^3q}{(2\pi)^3}\frac{4\pi e^2}{q^2\varepsilon(q)}\exp(iq\cdot r) = \frac{e^2}{i\pi r}\int_{-\infty}^{+\infty}dq\,\frac{\exp(iqr)}{q\varepsilon(q)} \tag{14}$$

and the integrand is non-analytic at $q = \pm 2k_F$: $1/[q\varepsilon(q)]_{q\to\pm 2k_F} \to -A[q \text{ m } 2k_F]\ln|\,q \text{ m } 2k_F\,|$ +regular terms , with $A = \kappa_{TF}^2/[4k_F^2(\kappa_{TF}^2 + 8k_F^2)]$. Hence,

$$V_H(r)\big|_{r\to+\infty} = -\frac{Ae^2}{i\pi r}\int_{-\infty}^{+\infty}dq\exp(iqr)[(q-2k_F)\ln|\,q-2k_F\,| + (q+2k_F)\ln|\,q+2k_F\,|]$$

$$= -\frac{2Ae^2}{r^3}\cos(2k_Fr). \tag{15}$$

This result is based on a theorem on Fourier transforms, stating that the asymptotic behavior of $V_H(r)$ is determined by the low-q behavior as well as by the singularities of $V_H(q)$. Obviously, in the present case the asymptotic contribution from the singularities is dominant over the exponential decay of Thomas-Fermi type coming from low q. The result in Eq. (15) implies that the screened ion-ion interaction in a metal has oscillatory character and ranges over several shells of neighbors, as has been observed experimentally.

(c) *Dependence of static screening on dimensionality*. Consider now a system in which the conduction electrons are restricted to move along a line. The Fermi surface reduces to two planes located at $k = \pm k_F$ and the elastic scattering processes (with energy transfer $\omega = 0$) can occur only with momentum transfer $q = 0$ or $q = 2k_F$. A window of forbidden excitations opens in the scattering spectrum at low energies: in $1D$ the excitations having $\omega \le |\,\omega_2(q)\,|$ in the range $0 \le q \le 2k_F$ are forbidden. A full calculation yields

$$S_0(q,\omega) = \frac{2\pi}{qv_F} \quad for\ |\,\omega_2(q)\,| \le \omega \le \omega_1(q) \tag{16}$$

and zero otherwise. Hence,

$$\chi_0(q) = -\frac{2m}{\pi\hbar^2q}\ln\left|\frac{q+2k_F}{q-2k_F}\right|. \tag{17}$$

The singularities at the edges of the continuum are stronger than in $3D$ and the singularity of the static response at $q = \pm 2k_F$ is a logarithmic divergence in $\chi_0(q)$ rather than in its derivative.

This behavior of static screening in 1D drives the *Peierls distortion* [7] in low-dimensional conductors: *e.g.* a monatomic 1D conductor with a half-filled conduction band gains electronic energy by a lattice distortion opening a gap at the Fermi level through the formation of dimers. Fig. 2 illustrates the dependence of $\chi_0(q)$ on dimensionality.

We conclude this discussion by giving the general expressions for the spin-resolved response of the ideal Fermi gas. These are

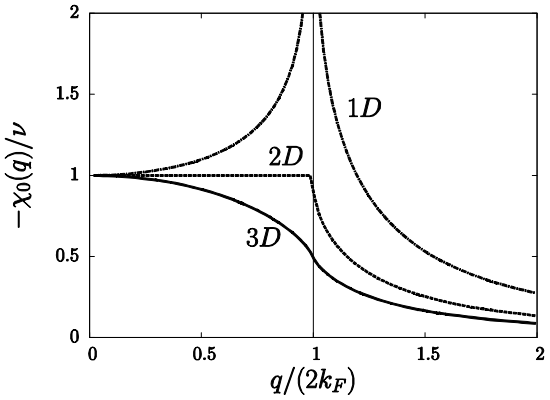

Figure 2. Illustrating the dimensionality dependence of the static density response of the ideal Fermi gas.

$$\chi^0_{zz}(q,\omega)=\sum_p[\frac{n^0_{p+q,\uparrow}-n^0_{p,\uparrow}}{\omega-(e_{p+q,\uparrow}-e_{p,\uparrow})+i\eta} + \frac{n^0_{p+q,\downarrow}-n^0_{p,\downarrow}}{\omega-(e_{p+q,\downarrow}-e_{p,\downarrow})+i\eta}], \tag{18}$$

and

$$\chi^0_{-+}(q,\omega)=\sum_p\left[\frac{n^0_{p+q,\uparrow}-n^0_{p,\downarrow}}{\omega-(e_{p+q,\uparrow}-e_{p,\downarrow})+i\eta}\right]. \tag{19}$$

In the paramagnetic state neither the single-particle energies nor the momentum distributions depend on spin orientation and hence $\chi^0_{zz}(q,\omega)=2\chi^0_{-+}(q,\omega)=\chi_0(q,\omega)$, with $\chi_0(q,\omega)$ being again the Lindhard free-electron response. In the static case one recovers at long wavelengths the Pauli susceptibility $\chi^0_{zz}(q\to 0,0)=\chi_0(q\to 0,0)\propto\nu$ for free electrons, where ν is again the density of states at the Fermi level. Short-range correlations (which are neglected in the RPA) play a crucial role in the spin response of an interacting EG, since the application of a magnetic field does not induce charge separation in the RPA sense.

2.4. Analytic theory of pair correlation function for 3D EL

We consider an inhomogeneous 3D fluid of electrons consisting of the two spin species with densities $n_\sigma(r)$ in the presence of external potentials $V^{ext}_\sigma(r)$ and of a uniform neutralizing background. From the Hohenberg-Kohn theorem[8] the ground-state energy functional of the fluid can be written as

$$E_{gs}[\{n_\sigma(r)\}]=T_s[\{n_\sigma(r)\}]+\sum_\sigma\int d^3r V^{ext}_\sigma(r)\Delta n_\sigma(r) + E_H[\{n_\sigma(r)\}]+E_{xc}\{n_\sigma(r)\}], \tag{20}$$

where $\Delta n_\sigma(r)=n_\sigma(r)-n_\sigma$ are the deviations of the spin densities from their average values, T_s and E_{xc} are the ideal kinetic energy and exchange-correlation energy functionals, and E_H is the Hartree term given by

$$E_H[\{n_\sigma(r)\}]=\frac{1}{2}\sum_{\sigma,\sigma'}\int d^3r\int d^3r' v(|r-r'|)\Delta n_\sigma(r)\Delta n_{\sigma'}(r') \tag{21}$$

with $v(|r-r'|)=e^2/|r-r'|$. Similar idea has been used before by our group [9]. The Euler-Lagrange equations for the spin-resolved pair functions can now be obtained from the variational principle of Hohenberg and Kohn[8] using the von Weizsäcker-Herring ideal kinetic energy functional. With the zero of energy taken at the chemical potential, the formally exact differential equation for $g_{\sigma\sigma'}(r)$ reads

$$\left[-\frac{\hbar^2}{m}\nabla^2_r+v(r)+v^{\sigma\sigma'}_P(r)+V^{\sigma\sigma'}_{ex}(r)\right]\sqrt{g_{\sigma\sigma'}(r)}=0. \tag{22}$$

The correlation functional would also become relatively negligible in the limit $r_s\to 0$. One way to defined $v^{\sigma\sigma'}_P(r)$ is

$$v^{\sigma\sigma'}_P(r)=\frac{\hbar^2}{m}\frac{\nabla^2_r\sqrt{g^{HF}_{\sigma\sigma'}(r)}}{\sqrt{g^{HF}_{\sigma\sigma'}(r)}}, \tag{23}$$

in the weak coupling limit $r_s\to 0$. In Eq. (23) $g^{HF}_{\sigma\sigma'}(r)$ are the spin-resolved pair functions in the Hartree-Fock approximation and $k_{F\sigma}=k_F(1+sgn(\sigma)\zeta)^{1/3}$ and $\zeta=|n_\uparrow-n_\downarrow|/n$ the degree of spin polarization.

The Fermi-hypernneted chain approach (FHNC) expresses the potential $V^{\sigma\sigma'}_{ex}(r)$ in Eq. (22), which is the sum of the Hartree and of the exchange-correlation potential, as the sum of two effective pair interactions:[10, 11, 12, 13]

$$V^{\sigma\sigma'}_{ex}(r)=W^{\sigma\sigma'}_B(r)+\delta_{\sigma\sigma'}W^{\sigma\sigma}_e(r). \tag{24}$$

Minimization of the ground state energy against arbitrary variations of $g_{\sigma\sigma'}(r)$ yields the expression

$$W^{\sigma\sigma'}_B(q)=-\frac{\varepsilon_q}{\sqrt{n_\sigma n_{\sigma'}}}[S_{\sigma\sigma'}(q)-\delta_{\sigma\sigma'}]-V_{\sigma\sigma'}(q) \tag{25}$$

where $\varepsilon_q=\hbar^2q^2/(2m)$ are the single-particle kinetic energies and the functions $V_{\sigma\sigma'}(q)$ are given by

$$\begin{cases} V_{\sigma\sigma}(q)=\dfrac{\varepsilon_q}{2n_\sigma}\left\{-1+[S^2_{\bar\sigma\bar\sigma}(q)+S^2_{\sigma\bar\sigma}(q)]/\Delta^2(q)\right\} \\ V_{\sigma\bar\sigma}(q)=-\dfrac{\varepsilon_q}{2\sqrt{n_\sigma n_{\bar\sigma}}}S_{\sigma\bar\sigma}(q)[S_{\sigma\sigma}(q)+S_{\bar\sigma\bar\sigma}(q)]/\Delta^2(q) \end{cases} \tag{26}$$

with

$$\Delta(q)=S_{\sigma\sigma}(q)S_{\bar\sigma\bar\sigma}(q)-S^2_{\sigma\bar\sigma}(q), \tag{27}$$

where $S_{\sigma\sigma'}(q)$ is spin dependence static structure function defined so that $S_{\sigma\sigma'}(q)=\delta_{\sigma,\sigma'}+FT[g_{\sigma\sigma'}(r)-1]$. The Fourier transformation is defined according to the general expression

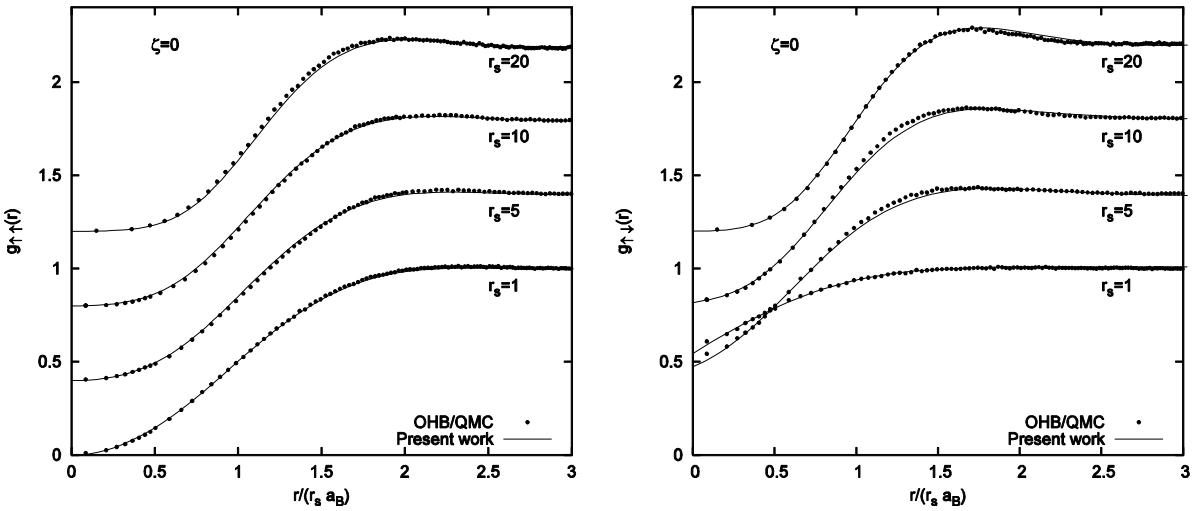

Figure 3. The spin resolved pair distribution function $g_{\uparrow\uparrow}(r)$ (panel left) and $g_{\uparrow\downarrow}(r)$ (panel right) in a paramagnetic $3D$ EG at $r_s = 1,5,10$ and 20, as a function of $r/(r_s a_B)$. The results of the present work (full lines) are compared with QMC data of Ortiz *et al.* [15] (dots). The curves at $r_s = 5,10$ and 20 have been shifted upwards for clarity by 0.4, 0.8 and 1.2, respectively. For more details see Davoudi *et al* [16]

$FT[F_{\sigma\sigma'}(r)] = \sqrt{n_\sigma n_{\sigma'}}\int dr F_{\sigma\sigma'}(r)\exp(ik\cdot r)$. Equations (26)-(27) show how the effective boson-like interactions $W_B^{\sigma\sigma'}(r)$ in Eq. (24) are related in Fourier transform to the spin-resolved pair distribution functions.

Turning to the second term on the left-hand side of Eq. (25), the effective pair potential $W_e^{\sigma\sigma}(r)$ has a very complicated expression within the FHNC.[10, 11, 12] However, in dealing with a one-component electron fluid Kallio and Piilo[14] have proposed a simple and effective way to account for this consequence of the antisymmetry of the fermion wave function. Their argument is immediately generalized to our two-component Fermi fluid, and leads to the requirement that in Fourier transform this term should cancel the effective boson-like interaction $W_B^{\sigma\sigma}(q)$ for parallel-spin electrons at low coupling. That is,

$$W_e^{\sigma\sigma}(q) = -\lim_{r_s\to 0} W_B^{\sigma\sigma}(q) = \frac{\varepsilon_q}{2n_\sigma}[1 + 2\,S_{\sigma\sigma}^{HF}(q)]\left[\frac{S_{\sigma\sigma}^{HF}(q)-1}{S_{\sigma\sigma}^{HF}(q)}\right]^2 \tag{28}$$

Here, $S_{\sigma\sigma}^{HF}(q)$ is the Hartree-Fock structure factor.

It is evident that the insertion of Eqs. (23)-(27) into Eq. (22) allows a self-consistent calculation of the spin-resolved pair distribution functions and of the effective electron-electron interactions.

In Figure 3 we show that our results for $g_{\uparrow\uparrow}(r)$ and $g_{\uparrow\downarrow}(r)$ in the paramagnetic EG at $r_s = 1,5,10$ and 20 are in excellent agreement with the quantum Monte Carlo (QMC) data of Ortiz *et al.*[15]. In the same range our results for $g(r)$ are in excellent agreement with those of Kallio and Piilo.[14] To the best of our knowledge theoretical results of similar quality have not been reported in the literature from an approach which is free of input and/or fitting parameters.

3. Extend the FHNC approach for 2D EL

In above we have presented an analytic theory of $g(r)$ and other ground-state properties of the 3D electron gas [16]. The theory was based on a Fermi hypernetted chain approximation (hereafter indicated by the FHNC/0 acronym) and yields quantitative agreement with QMC data up to at least $r_s = 20$. The object of this part is to extend the theory of $g(r)$ and the correlation energy to the 2D electron gas. As we shall see, much higher sophistication is needed to attain a quantitatively useful theory in lowered dimensionality. We shall have to dwell on terms beyond the FHNC/0, which come from low-order elementary diagrams and from three-body Jastrow-Feenberg correlations.

As in Ref. [16] we split the ideal kinetic energy functional into the sum of the von Weizsäcker - Herring term $(\hbar^2/8m)\int dr|\nabla n(r)|^2/n(r)$ and a residue $T_\theta[n(r)]$, and minimize the energy by means of the Hohenberg-Kohn variational principle. The result is a differential equation for $\sqrt{g(r)}$,

$$[-\frac{\hbar^2}{m}\nabla^2 + v(r) + W_F(r) + W_B(r)]\sqrt{g(r)} = 0. \tag{29}$$

The FHNC/0 and its HNC/0 equivalent for a Bose fluid [17, 18, 19] take

$$W_B^{HNC}(k) = -\frac{\hbar^2 k^2}{4m}\left[\frac{S(k)-1}{S(k)}\right]^2[2S(k)+1], \tag{30}$$

where $W_B(k)$ is the Fourier transform of $W_B(r)$. Using Eq. (30) in Eq. (24) with $W_F(r) = 0$ and self-

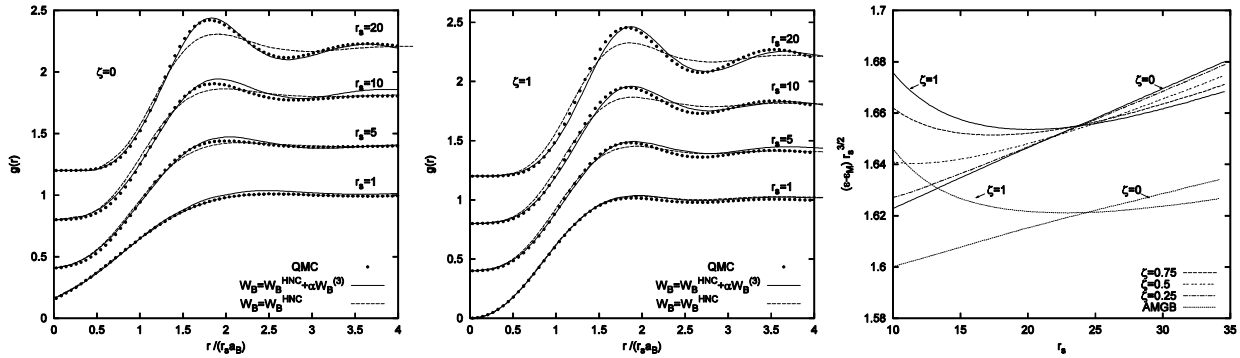

Figure 4. The pair distribution function $g(r)$ of the 2D electron gas at $r_s =$ 1, 5, 10, and 20 in the paramagnetic state (Left panel) and in the fully spin-polarized state (Middle panel), as a function of distance (in units of $r_s a_B$). The theoretical results (full lines) are compared with QMC data by Gori-Giorgi *et al.* [21] (dots). The dashed lines show the results obtained in the FHNC/0 scheme. The results have been shifted upwards by 0.4, 0.8 and 1.2 for clarity. The ground-state energy of the $2D$ electron gas (in Rydberg units, referred to the Madelung energy $\varepsilon_M = -2.2122 / r_s$ and multiplied by $r_s^{3/2}$) as a function of the coupling strength r_s (Right panel). The full lines show the theoretical results for the paramagnetic state and the fully spin-polarized state, while the dots report QMC data from Attaccalite *et al*. [22]. The other three curves are theoretical results for states of partial spin polarization, as indicated in the figure. For more details see Asgari *et al* [23].

consistently solving Eq. (29) for $g(r)$, we find quantitative agreement with the QMC data of Ref. [20] at $r_S = 1$ and discrepancies already emerging at $r_S = 5$.

Improvements on Eq. (30) can be sought in two directions for a Bose fluid. The HNC may be transcended by the inclusion of low-order elementary diagrams, and three-body Jastrow-Feenberg correlations may be included. The contribution from the first elementary diagrams to the effective Bose potential is

$$W_B^{E_4}(k) = -\frac{\hbar^2}{4mn}\left\{\frac{k^2}{(2\pi)^2}\varepsilon_4(k) + \int\frac{dq}{(2\pi)^2}q^2[S(q)-1]\frac{\delta\varepsilon_4(q)}{\delta S(k)}\right\}, \tag{31}$$

where $\varepsilon_4(k)$ is given by a fourfold integral (in 2D) over momentum space. The contribution of three-body correlations is given by a two-fold integral,

$$W_B^{(3)}(k) = \frac{1}{4n(2\pi)^2}\int dqS(p)S(q)u_3(q,p,k)\{v(q,p,k) + \left[\varepsilon(p)+\varepsilon(q)\right]u_3(q,p,k)\} \tag{32}$$

where $p = -(q+k)$, $\varepsilon(k) = \hbar^2k^2/[2mS(k)]$ and, with the definition $X(k) = 1 - S^{-1}(k)$, we have $v(q,p,k) = (\hbar^2/m)[k\cdot pX(p) + k\cdot qX(q) + p\cdot qX(p)X(q)]$ and

$$u_3(q,p,k) = -(\hbar^2/2m)\times \frac{[k\cdot pX(p)X(k) + p\cdot qX(p)X(q) + k\cdot qX(q)X(k)]}{\varepsilon(k)+\varepsilon(p)+\varepsilon(q)} \tag{33}$$

The papers of Smith *et al*. [19] and of Apaja *et al*. [18] should be consulted for detailed derivations of these equations, in which $u_3(q,p,k)$ is the irreducible three-body vertex.

We tried to take into account the higher-order terms that are missed in these approaches at strong coupling by assuming that they lead to corrections in the scattering potential that have roughly the same shape as the low-order terms reported above. In particular, we found that the choice

$$W_B^{(\alpha)}(r) = W_B^{HNC}(r) + \alpha(r_S)W_B^{(3)}(r), \tag{34}$$

leads to a satisfactory account of the QMC data on the 2D Bose gas. Here the parameter α is determined by fitting the QMC data on the ground-state energy [20] with a relative precision of 10^{-3}. This yields

$$\alpha(r_S) = 1 + 5.888\exp(-0.07758\, r_S^{0.7923}). \tag{35}$$

An important requirement is that Eq. (29) should give the exact fermion-fermion distribution function when one goes to the weak-coupling limit $r_S \to 0$, when $g(r)$ becomes the Hartree-Fock pair distribution function $g_{HF}(r)$. The Fermi term in the scattering potential is then determined by the Hartree-Fock structure factor $S_{HF}(k)$ according to

$$W_F(k) = \frac{\hbar^2}{m}FT\left[\frac{\nabla^2\sqrt{g_{HF}(r)}}{\sqrt{g_{HF}(r)}}\right] + \frac{\hbar^2k^2}{4m}\left[\frac{S_{HF}(k)-1}{S_{HF}(k)}\right]^2[2S_{HF}(k)+1] - \alpha(r_S)W_B^{(3)}(k)\,|_{S(k)=S_{HF}(k)}\,. \tag{36}$$

Our numerical results for the pair distribution function of the 2D electron gas in the paramagnetic state ($\zeta = 0$) and in the fully spin-polarized state ($\zeta = 1$) are compared with the QMC data of Ref. [21] in Fig. 4. We clearly achieved fully quantitative agreement with the QMC data up to large values of the coupling strength r_S.

We can then confidently calculate the ground-state energy $\varepsilon(r_s,\zeta)$ of the 2D electron gas as a function of r_S in these two states of magnetization, using an integration over the coupling strength according to the expression

$$\varepsilon(r_s,\zeta)=\frac{(1+\zeta^2)}{r_s^2}+\frac{1}{2}\int_0^1\frac{d\lambda}{\lambda}\int\frac{dk}{(2\pi)^2}v_k^{(\lambda)}[S_\lambda(k)-1] \tag{37}$$

(in Rydberg units). The results are compared with the QMC data of Attaccalite *et al*. [22] in Fig. 4, right panel. There clearly is a discrepancy with the data in the absolute values of the energy, but this affects in essentially the same manner the two phases so that we find a transition from the paramagnetic to the fully spin-polarized fluid at $r_S \approx 24$, in excellent agreement with the QMC data. As to the nature of the phase transition, within the accuracy of our calculations it could be either a weakly first-order one or a continuous transition occurring in an extremely narrow range of values of r_S. This is shown in Fig. 4, where we also report our results for the ground-state energy as a function of r_S at several values of the spin polarization ζ.

Consequently, we present a model which quantitatively predicts the two-body correlations in both the 2D charged-boson fluid and the 2D electron gas using as the only input the QMC data for the ground-state energy of the boson fluid as a function of the coupling strength r_S. The essential physical idea that underlies the model is that differences arising from the statistics are disappearing as the fermionic or bosonic fluid is brought into the strong coupling regime, where the Coulomb repulsions suppress close encounters of pairs of particles. However, exchange between parallel-spin fermions must be properly accounted for in the weak-to-intermediate coupling regime. The model has allowed us to reproduce the quantum phase transition that has been found to occur in the QMC studies of the 2D electron gas, essentially starting from the basic Coulomb Hamiltonian. Within the accuracy of our model the transition could be either a weakly discontinuous transition or a continuous one occurring in a very narrow range of coupling strength.

3.1. Quasiparticle properties of two-dimensional electron liquid

Theoretical calculations of the effective mass and spin-susceptibility of electron systems are performed within the framework of Landau's Fermi liquid theory [24] whose key ingredient is the quasiparticle concept and its interactions. Among the methods designed to deal with the intermediate density regime, of particular interest for its physical appeal and elegance is Landau's phenomenological theory [24] dealing with low-lying excitations in a Fermi liquid. Landau called such single-particle excitations quasiparticles and postulated a one-to-one correspondence between them and the excited states of a noninteracting Fermi gas. He wrote the excitation energy of the Fermi-liquid in terms of the energies of the quasiparticles and of their effective interaction. The quasiparticle-quasiparticle interaction function can, in turn, be used to obtain various physical properties of the system and can be parametrized in terms of experimentally measurable data.

As applied to the electron gas model this entails the calculation of effective electron-electron interactions which enter the many-body formalism allowing the calculation of various physical properties. A number of calculations considered different variants of the GW - approximation for the self-energy[25, 26, 27, 28, 29, 30, 31] from which density, spin-polarization, and temperature dependence of effective mass are obtained. In these calculations the on-shell approximation[27, 28] yields a diverging effective mass but the full solution of Dyson equation yields only a mild enhancement.[30, 31] Other approaches exploiting the similarity to neutral fluid ^{3}He in the vicinity of MIT a found diverging effective mass.[32, 33]

We consider a theory in which the layer thickness effects enter the local-field factors. In this direction, we use accurate static structure factors resulting from a Fermi hypernetted-chain self-consistent calculation [10, 11, 12] (FHNC) in conjunction with the fluctuation-dissipation theorem to extract the local-field factors which depend on the quantum-well width. We find that for the specific sample parameters of Tan *et al*.[34] good agreement between the experimentally observed spin-susceptibility and our theoretical results can be achieved up to the intermediate coupling strength regime. Our results are also in good agreement with the QMC simulations of De Palo *et al*.[35] in the same range of coupling strengths implying the efficacy of our theoretical approach.

To calculate the quasiparticle (QP) properties, we start with the calculation of the retarded self-energy, which can be decomposed in the usual way into the frequency independent Hartree-Fock and frequency dependent correlation parts.[26, 28] The correlation part of the self-energy involves the effective QP interaction between the electrons for which we use the Kukkonen-Overhauser form.[26, 37] The main ingredient of this formalism is the screening dielectric function

$$\frac{1}{\varepsilon(q,\omega)}=1+v_q[1-G_+(q)]^2\chi_C(q,\omega)+3v_qG_-^2(q)\chi_S(q,\omega).$$

In this expression $\chi_C(q,\omega)$ and $\chi_S(q,\omega)$ represent the charge-charge and spin-spin response functions, which in turn define and are determined by the spin-symmetric and spin-antisymmetric local-field factors $G_+(q)$ and $G_-(q)$ via the relations

$$\chi_{C,S}(q,\omega)=\frac{\chi_0(q,\omega)}{1-f_{C,S}(q)\chi_0(q,\omega)}, \tag{39}$$

where $f_C(q)=v_q[1-G_+(q)]$, $f_S(q)=-v_qG_-(q)$ and $\chi_0(q,\omega)$ is the response function of a noninteracting

system. In the paramagnetic electron liquid $G_{\pm}(q) = [G_{\uparrow\uparrow}(q) \pm G_{\uparrow\downarrow}(q)]/2$, where $G_{\sigma\sigma'}(q)$ are the spin-resolved local-field factors. Note that we have approximated the local-field factors by their static, frequency-independent limits. As we explained in the Hartree-Fock the pair distribution function gives the local structure as merely due to exchange between electrons with parallel spins, Pauli hole, the Coulomb repulsion induce additional local structure mainly through correlations between electrons with antiparallel spins, Coulomb hole. Therefore, because of the Pauli-Coulomb or precisely exchange-correlation hole, the local density of polarizable electron liquid around an electron is lower that the average density n. Hence, the Pauli-Coulomb hole has a direct role in determining the local-field factors.

Quite generally, once the QP self-energy is known, the QP excitation energy $\delta \mathrm{E}_{QP}(k)$, which is the QP energy measured from the chemical potential μ of the interacting system, can be calculated by solving self-consistently the Dyson equation

$$\delta \mathrm{E}_{QP}(k) = \xi_k + \Re e \sum\nolimits_{ret}^{R}(k,\omega)\Big|_{\omega=\delta \mathrm{E}_{QP}(k)/\mathrm{h}}, \qquad (40)$$

where $\Re\Sigma_{ret}^{R}(k,\omega) = \Re e\Sigma_{ret}(k,\omega) - \Sigma_{ret}(k_F,0)$. For later purposes we introduce at this point the so-called on-shell approximation (OSA). This amounts to approximating the QP excitation energy by calculating $\Re e\Sigma_{ret}^{R}(k,\omega)$ in Eq. (40) at the frequency $\omega = \xi_k/\mathrm{h}$.

Once the QP excitation energy is known, the effective mass $m^*(k)$ can be calculated by means of the relationship

$$\frac{1}{m^*(k)} = \frac{1}{\mathrm{h}^2 k}\frac{d\delta \mathrm{E}_{QP}(k)}{dk}. \qquad (41)$$

Evaluating the $m^*(k)$ at $k = k_F$, one gets the QP effective mass at the Fermi surface. We remark that the QP excitation energy may be calculated either by solving self-consistently the Dyson equation or using the OSA [40].

Starting with the quasiparticle energy and its relation to the Landau interaction function, one can drive the modified Landé g^* -factor expression. [26]

$$\frac{g}{g^*} = 1 + \frac{m^*}{2\pi}\int_0^{2\pi}\frac{d\phi}{2\pi}\left(\frac{\delta^2 E}{\delta n_k^{\uparrow}\delta n_p^{\uparrow}} - \frac{\delta^2 E}{\delta n_k^{\uparrow}\delta n_p^{\downarrow}}\right), \qquad (42)$$

where E is the total ground state energy. Here $|k| = |P| = k_F$ and ϕ is the angle between them. Once the QP effective mass m^* and modified Landé g^* -factor have been calculated the spin susceptibility is found by the following exact relationship

$$\frac{\chi^*}{\chi_0} = \frac{m^*}{m}\frac{g^*}{g}, \qquad (43)$$

where χ_0 is the Pauli spin susceptibility.

As is clear from Eqs. (38, 39) the local-field factors are the fundamental quantities for an evaluation of quasiparticle properties. Our strategy is to use accurate spin-symmetric and spin-antisymmetric static structure factors to build the local-field factors.[38] For this purpose we use the Fermi hypernetted-chain approach [10, 11, 12, 13] to calculate the spin-symmetric and spin-antisymmetric static structure factors incorporating the finite thickness effects in a quantum well.

The fluctuation-dissipation theorem relates the dynamic susceptibilities defined above to the static structure factors

$$S_{\pm}(q) = -\frac{1}{n\pi}\int_0^{\infty} d\omega \Im m[\chi_{C,S}(q,\omega)], \qquad (44)$$

where $S_{\pm}(q) = \left[S_{\uparrow\uparrow}(q) \pm S_{\uparrow\downarrow}(q)\right]/2$. As $\chi_C(q,\omega)$ and $\chi_S(q,\omega)$ depend on $G_+(q)$ and $G_-(q)$, respectively, the above integral expression allows one to determine the local-field factors once the static structure factors are calculated by the FHNC approach.

To assess the validity of our procedure, we first show the calculated pair-distribution function $g(r)$ at two representative values of $r_s = 3$ and $r_s = 6$ in Fig. 5, left panel. For the strictly 2D system we compare our $g(r)$ with that obtained by Gori-Giorgi *et al.*[21] from QMC simulations. For these intermediate densities we find very good agreement and the omission of bridge diagrams within the FHNC is justified *a posteriori*. Figure 5 also shows our results for a Q2D EG. The effect of finite thickness on $g(r)$ is more appreciable for small values of r_s.

We note that there are qualitative differences at small distances and in particular the on-top value $g(0)$. It is not clear at this point whether these differences are because of the neglect of bridge functions in our implementation of the FHNC calculation or not. QMC simulations for Q2D EG would help establish the correct behavior of $g(r)$ for finite thickness samples.

We next display the local-field factors $G_+(q)$ and $G_-(q)$ calculated within the present approach in comparison to those constructed by Davoudi *et al.*[36] using the QMC data and known sum-rules. Our local-field factors typically start at zero in the long-wavelength limit and go to a constant for large values of q as shown in Fig. 5. The main qualitative difference between our $G_+(q)$ and $G_-(q)$ and the Davoudi *et al.*[36] construction is in the large q behavior. In particular, a peak structure both in $G_+(q)$ and $G_-(q)$ occurring around $q \approx 3k_F$ and $q \approx 2k_F$, respectively, is quite well reproduced. Our local-field factors satisfy the fluctuation-dissipation theorem but not the compressibility sum-rule, whereas those of Davoudi *et al.*[36] satisfy the compressibility sum-rule but not the fluctuation dissipation theorem. In fact, it is known that frequency dependent (dynamical) local-field factors are

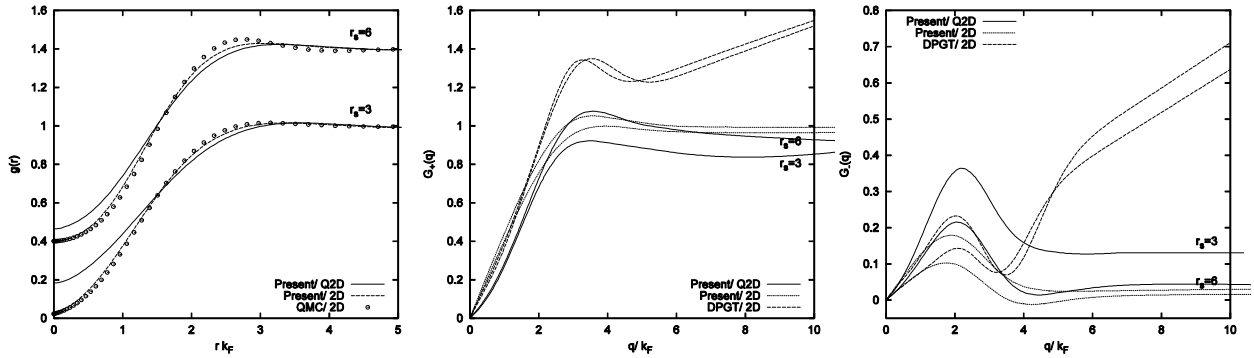

Figure 5. (Left panel) Pair-correlation function $g(r)$ for $r_S = 3$ (lower curves) and $r_S = 6$ (upper curves has been shifted upwards by 0.4). Symbols are QMC results of Gori-Giorgi *et al*. Ref. [21] for a strictly 2D electron gas, dashed and solid lines are those calculated within the present approach for 2D and Q2D EG, respectively. (Middle Panel) The local-field factors $G_+(q)$ as a function of q / k_F for $r_S = 3$ and $r_S = 6$. Note that $G_+(q \to \infty)$ tends to a larger constant value with increasing r_S. (Right Panel) The local-field factors $G_-(q)$ as a function of q / k_F for $r_S = 3$ and $r_S = 6$. In both figures, dashed lines are analytical expression of QMC results of Davoudi *et al*. Ref. [36] for a strictly 2D electron gas, dotted and solid lines are those calculated within the present approach for 2D and Q2D EG, respectively. Note that $G_-(q \to \infty)$ tends to a smaller constant value with increasing r_S. For more details see Asgari and Tanatar [40]

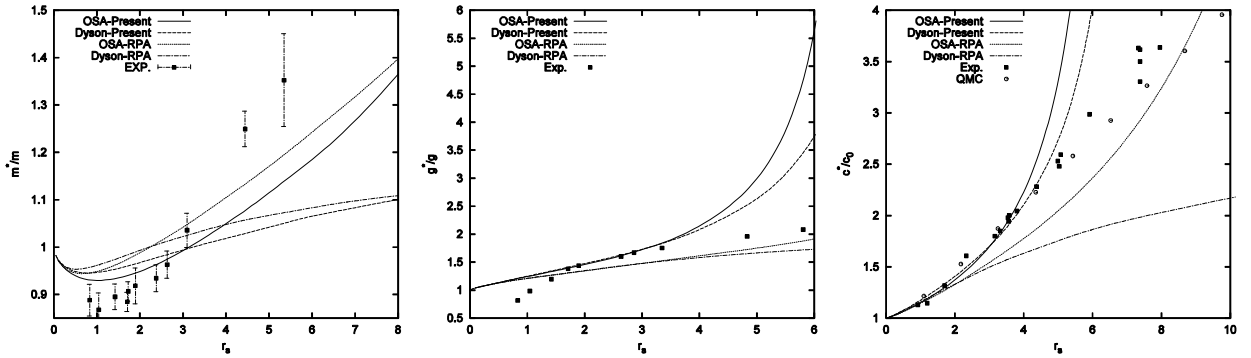

Figure 6. (Left panel) Many-body effective mass as a function of r_S for $0 \le r_S \le 8$ for a Q2D electron gas confined in a GaAs/AlGaAs triangular quantum well of the type used in Ref.[34]. (Middle panel) g^* / g as a function of r_S for $0 \le r_S \le 6$. The experimental data $\chi^* m / \chi_0 m^*$ is from the χ^* / χ_0 of empirical formula given by Ref.[tan] divided by the m^* / m of Ref.[39]. (Right panel) spin susceptibility as a function of r_S for $0 \le r_S \le 10$ for a Q2D electron gas confined in a GaAs/AlGaAs triangular quantum well of the type used in Ref.[39] compared with quantum Monte Carlo results of Ref. [35]. For more details see Asgari *et al* [40]

needed to fulfill both requirements.

In Fig. 6, left panel we show our numerical results of the QP effective mass both in OSA and Dyson approximations. The QP effective mass enhancement is substantially smaller in the Dyson equation calculation than in the OSA. Comparing the results of Fig. 6 with the experimental measurements of Tan *et al*.[34] we can draw the following conclusions: (i) The RPA and present results are rather similar in the weak coupling limit ($r_S << 1$), (ii) theoretical calculations in the strong coupling region are not so close to experimental data. There is an essential point which we should stress here that experimental data were collected at weak magnetic fields and mostly in high Landau levels, however our numerical calculations have been performed in the absence of a magnetic field. Figure 6, middle panel depicts our results for the ratio g^* / g as a function of r_S for $0 \le r_S \le 6$. g^* / g is calculated from Eq. (16) and embodies the charge and spin fluctuation effects through G_+ and G_-. We included the value of experimental $\chi^* m / \chi_0 m^*$ which is extracted from the χ^* / χ_0 empirical formula given by Tan *et al.* [39] divided by the experimental data of m^* / m of Tan *et al*. [34]. We observe that there is an enhancement in g^* beyond r_S : 5 within the present method using either OSA or the Dyson approaches compared to the experimental data and the RPA calculation. In particular, it is surprising that RPA yields a reasonable agreement with experiment in a region of r_S values where it is not expected to be very reliable. In Fig. 6, right panel we show the spin susceptibility as a function of r_S compared to RPA, recent experimental data of Zhu *et al*.[39] and quantum Monte Carlo calculation [35]. As it is clear from this figure χ^* / χ starts at unity when r_S

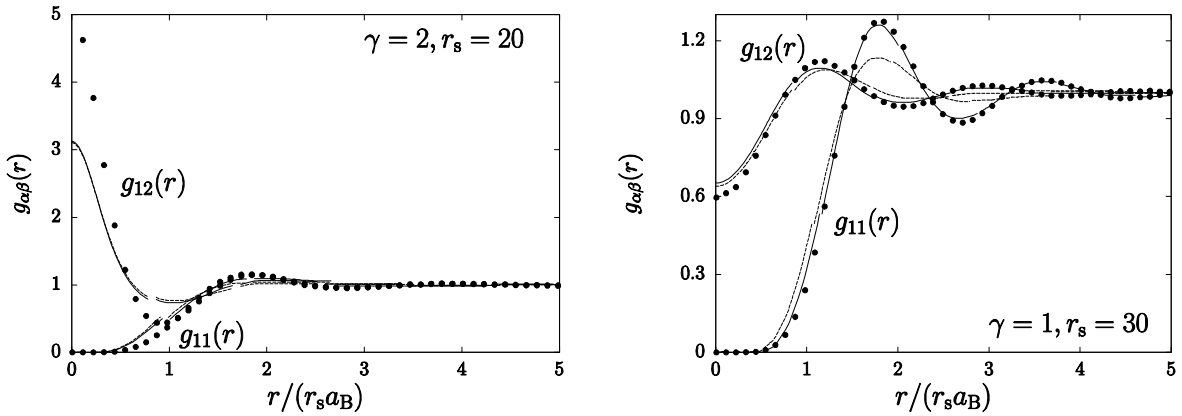

Figure 7. The pair distribution functions $g_{\alpha\beta}(r)$ in a symmetric e-h (Left panel) bilayer at $\gamma \equiv 2(r_s a_B)/d$ and $r_s = 20$, as a function of $r/(r_s a_B)$. The results of FHNC/$\mathcal{J}3$ (solid lines) are compared with FHNC/0 (dashed lines) and DMC data[44](dotes). The pair distribution functions $g_{\alpha\beta}(r)$ in a symmetric e-e (right panel) bilayer at $\gamma \equiv (r_s a_B)/d$ and $r_s = 30$, as a function of $r/(r_s a_B)$. The results of FHNC/$\mathcal{J}3$ (solid lines) are compared with FHNC/0 (dashed lines) and DMC data[44](dotes). For more details see Abedpour *et al* [45]

tends to zero and increases with increasing r_s values. Our numerical calculations within both OSA and Dyson approximations are in good agreement with the experimental measurements in the weak and intermediate coupling limits. Our numerical calculations are in better agreement with the QMC compared to the 2D EG case.

4. Ground-state properties of Electron-Hole Bilayer systems

The Electron-Hole Bilayer Systems (EHBS) have been center of experimental and theoretical investigation [41] for many years. The advances in the nanoscale semiconductor fabrication technology have made available these Fermi liquid system in the couple semiconductor quantum-well structures with a good control on the electron and hole density and the interwell spacing. The Coulomb attraction existing between the two kinds of fermions naturally brings about pairing, hence, the possibility of a coherent state [42]. It was realized [43] soon that system of spatially separated electrons and holes, such as a bilayer, have a number of advantages with respect to the conventional bulk sample [41] in which electrons and holes occupy the same region. Thus, while in a homogeneous semiconductor the excitonic condensate would be an insulator [42], in a bilayer superconducting phase is in principle possible [43].

We consider a double-quantum-well system with electrons in the first and holes in the second well, with masses m_1 and m_2, and densities n_1 and n_2 respectively. We suppose the confining potential of each layer to be so high and narrow that we can neglect any inter-layer tunneling and consider the motion of carriers in the two wells as purely two-dimensional. We take the distance d between the layers to be small in order to permit inter-layer interactions. The Hamiltonian of the system is

$$H = -\frac{\hbar^2}{2}\sum_{(i,\alpha)}\frac{\nabla^2_{i,\alpha}}{m_\alpha} + \frac{1}{2}\sum_{(i,\alpha)\neq(j,\beta)} v_{\alpha,\beta}(r_{ij}), \qquad (45)$$

where $v_{\alpha\alpha} = e^2/r$ and $v_{\alpha\bar{\alpha}} = -e^2/\sqrt{r^2+d^2}$ with (i,α) indicating the i-th particle in the layer α. Our aim is to calculate the pair correlation functions $g_{\alpha\beta}(r)$ of the e-h and e-e bilayers

$$g_{\alpha\beta}(r) = \frac{1}{S}\frac{1}{n_\alpha n_\beta}\sum_{(i,\alpha)\neq(j,\beta)}\left\langle \delta(r - r_{(i,\alpha)} + r_{(j,\beta)})\right\rangle, \qquad (46)$$

where the average is taken on the ground state and S is the area of the sample.

Fig. 7 reports our numerical results for the pair correlation functions $g_{\alpha\beta}(r)$ for different values of layer density r_s and interlayer separation $\gamma \equiv (r_s a_B)/d$ obtained within FHNC/0 and FHNC/$\mathcal{J}3$ approximations. Apart from a better agreement with QMC data in compare with previous local-field based results, it is also free of an instability which usually appears in that methods in the strong coupling regime (*i.e* large r_s and/or small interlayer separation d). Since the three-body correction inters just in the intra-layer component of the effective potential, the agreement between QMC data and our results for inter-layer pair correlation function in strong coupling is still poor, especially the on-top value of interlayer pair correlation function $g_{\alpha,\bar{\alpha}}(0)$ is always underestimated.

In the results, we present a self-consistent analytical theory of the intra-layer and inter-layer pair distribution functions $g_{\alpha\beta}(r)$ of electron-hole bilayer system. Our approach involves the solution of the zero energy scattering Schrödinger equation with an effective potential which includes a Bose-like term from Jasrow-Feenberg correlations and a Fermi term from exchange

and kinetic energy, tailored to include Hartree-Fock limit in high density. Our theory is also shown to satisfy plasmon sum rule and the charge neutrality condition. We obtain very good agreement with quantum Monte-carlo results for pair correlation functions over a wide range of densities and inter-layer distances. No instability observed in the wide range of parameters we have studied. For a better result in the strong coupling regime, and possible tracing of excitonic phase, the inter-layer correlation potential also needs to be improved.

4.1. Charge Coulomb drag effect in bilayer electron systems

In contrast to the single layer resistivity which shows a nontrivial interplay between interaction and disorder effects near the metal-insulator transition[46], the inter-layer resistivity is largely determined by the long range Coulomb scattering (as long as the single layer densities are away from metal-insulator transition region). Therefore Coulomb drag experiments provide valuable information on the intra- and inter-layer electron-electron interactions especially when the layer densities are lowered.

Over the years there has been a number of Coulomb drag experiments at zero magnetic field using different samples and probing different parameter regimes. The main parameters entering a drag experiment set-up are the layer density n which may be related to the dimensionless coupling strength r_S, the separation distance between the layers d and the Fermi temperature T_F. Hill *et al*.[47] measured drag resistivity ρ_D in an electron bilayer system at densities corresponding to $1.13 \hat{} \; r_S \hat{} \; 1.57$ and high temperatures $T : T_F$. The observed peak in ρ_D around $T \approx T_F / 2$ was attributed to the contribution of plasmons. In fact, the experimental results were regarded as an indirect evidence for the existence of acoustic and optical plasmons in a bilayer system.[48] Similar experiments were also performed by Noh *et al*.[49] confirming plasmon effects on the drag resistivity and revealing the importance of possible dynamic correlations even though the layer densities were such that $r_S \approx 1.48$ where the strong coupling effects are not expected. More recent experiments by Kellogg *et al*.[50] used samples with layer densities reaching $r_S \approx 4.3$ and $k_F d : 1$ where d is the center-to-center well separation. In contrast to the above experiments, Pillarisetty *et al*.[51] measured frictional drag between two dilute 2D hole layers in which the r_S values were in the range $19 \le r_S \le 39$.

On the theoretical side, the drag resistivity has first been formulated within the random-phase approximation (RPA) for the layer density-response functions and inter-layer effective interaction.[52,53] Here and most subsequent works treat the inter-layer effective interaction as given by the bare inter-layer Coulomb interaction screened by the bilayer system dielectric function. Importance of dynamical correlations is noticed even at the RPA level since the difference between the static and dynamic screening function brings quantitative changes to the drag resistivity.[52] At larger r_S values when the correlation effects become significant one should go beyond the RPA. One way to do this in a physically motivated way is through the local-field corrections to the RPA form of the screening function. The simplest form of the local-field corrections is the Hubbard approximation which was used by Hill *et al*.[47] to analyze their data. A much widely used local-field corrections are calculated within the self-consistent field approximation scheme of Singwi *et al*.[54] (STLS). They have been incorporated in the evaluation of the drag resistivity by S' wierkowski *et al*.[55]. In connection with the Kellogg *et al*. experiments[50], Yurtsever *et al*.[56] pointed out that STLS local-field corrections yield a poor representation and suggested the use of a different effective interaction originally developed by Kukkonen and Overhauser[57] and Vignale and Singwi.[58] Recently, Badalyan *et al*.[59] employed frequency dependent local-field corrections in the long-wavelength limit ($q \to 0$) obtained from dynamical exchange-correlation kernel in the context of density functional theory.

We consider a double-quantum-well structure with d as the center-to-center well separation such that there is no tunneling between them and L as the width of the quantum wells. Each layer is characterized by the dimensionless coupling constant $r_s a_B^* = 1/\sqrt{\pi n}$ where n is the areal density, $a_B^* = \mathrm{h}^2 \varepsilon / (m^* e^2)$ is the effective Bohr radius, ε and m^* being the background dielectric constant and electron band effective mass. Each layer has only one type of charge carrier, i.e. electrons, although our theoretical formulation could be applicable to hole-hole and electron-hole layers with suitable changes. In the case of electron-hole bilayers the prospect of formation of an excitonic state[60] and its detection through drag experiments[61] requires a new formulation of the effective inter-layer interaction which we do not address here. However, correlations in electron-hole bilayers and their effects on drag resistivity can be studied using the improved inter-layer models we shall describe below. The motion of the carriers is free along the xy plane and under the action of a double-well potential profile in the z-direction only the lowest subband in each quantum well is occupied. For this aim, temperature should be less than the difference between excited energy level and the ground state energy in quantum well. This yields $T < 3(r_s a_B^* / L)^2 T_F / 16$. Furthermore, the bilayer system is assumed to be embedded in a uniform neutralizing positive background charge. The unscreened Coulomb interaction potential, in Fourier space, between the electrons in kth and lth layers is given by

$v_{kl}(q) = v_q F_{kl}(qL)$. Here, $v_q = 2\pi e^2/(\varepsilon q)$ and F_{kl} are infinite quantum-well form factors taking the finite width effects into account which are given by [52]

$$F_{kk}(x) = \frac{3x + 8\pi^2/x}{x^2 + 4\pi^2} - \frac{32\pi^4[1-\exp(-x)]}{x^2(x^2+4\pi^2)^2}$$

$$F_{kl}(x) = \frac{64\pi^4 \sinh^2(x/2)}{x^2(x^2+4\pi^2)^2}\exp(-qd). \quad (47)$$

We note that most theoretical calculations[52, 48, 55] adopt the infinite quantum-well model to account for the width effects, whereas a better way would be to calculate the Coulomb matrix elements using envelope functions $\phi_n(z)$ determined self-consistently from the Poisson and Schrödinger equations.[62]

The drag resistivity (or as it is also called transresistivity) ρ_D of an electron system at temperature T has been obtained in a variety of theoretical models. These include diagrammatic perturbation theory [52, 63], the Boltzmann equation [48] and the memory function formalism [53, 55]. In a drag experiment one applies an electric field E_1 to layer 1 (drive layer) creating a current to flow with current density J_1. This sets up an electric field E_2 in layer 2 (drag layer) where no current is allowed to flow. The drag resistivity is defined as $\rho_D = E_2/J_1$ and the microscopic calculations relate this quantity to the rate of change of momentum between the layers, as electron-electron inter-layer interactions transfer momentum from the drive layer with carrier density n_1 to the drag layer with density n_2.

Theoretical considerations lead to the same expression for ρ_D in terms of the effective inter-layer interaction and the density-response function of the single layers. When the effective inter-layer interaction treated perturbatively, ρ_D is given as

$$\rho_D = -\frac{\hbar^2}{8\pi^2 e^2 n_1 n_2 k_B T} \times$$

$$\int_0^\infty q^3 dq \int_0^\infty d\omega \frac{|W_{12}(q,\omega)|^2 \, \Im m\chi_1^0(q,\omega,T)\, \Im m\chi_2^0(q,\omega,T)}{\sinh^2(\hbar\omega/2k_BT)}, \quad (48)$$

where $\chi_i^0(q,\omega)$, ($i = 1$ or 2) is the non-interacting linear response corresponding to the drive and drag layer which shows the charge density fluctuations in a given layer at finite temperature and $W_{12}(q,\omega)$ is the effective inter-layer interaction. Let us examine Eq. (48) in the limit where $T \to 0$. We can rewrite Eq. (48) following Hu[64]

$$\rho_D = \int_0^\infty d\omega \frac{1}{\sinh^2(\omega/2T)} H(\omega), \quad (49)$$

and suppose that there is a scaling behavior such that $H(\omega) \approx \omega^\alpha$ as $\omega \to 0$. Substituting this form into the above equation gives $\rho_D \approx T^\alpha$ when $\alpha > 1$ and becomes ∞ for $\alpha \le 1$. When $\alpha \le 1$, evidently perturbation theory breaks down and the above expressions are invalid. When $\alpha > 1$, perturbation theory is valid and scaling behavior of ρ_D indicates that in the weak-coupling regime, as $T \to 0$ the drag resistivity must go to zero faster than linearly in T.

An important ingredient which is needed to calculate ρ_D is the electron-electron inter-layer interaction, $W_{12}(q,\omega)$. The effective electron-electron interaction for a two-component system given by a 2×2 matrices and in random-phase approximation (RPA) it is given by

$$\hat{W}_{RPA}(q,\omega) = \hat{v}(q) + \hat{v}(q)\hat{\chi}(q,\omega)\hat{v}(q), \quad (50)$$

where $\hat{\chi}(q,\omega)$ defined in terms of the non-interacting charge-charge response function and Coulomb interactions.

To take into account the effect of correlations more clearly, which are more important in the strongly correlated regime where r_s becomes large, we need more sophisticated approaches. For this purpose, we introduce here other approximation scheme for $W_{12}(q,\omega)$ proposed by S′wierkowski *et al*. [55, 59] (SSG) where

$$\hat{W}_{SSG}(q,\omega) = \hat{v}_{eff}(q) + \hat{v}_{eff}(q)\hat{\chi}(q,\omega)\hat{v}_{eff}(q), \quad (51)$$

where $v_{eff}^{ij}(q) = v_{ij}(q)(1 - G_{ij}(q))$ are the effective Coulomb interactions and $G_{ij}(q)$ are intra- and inter local-field corrections (LFC) which take into account multiple scattering to infinite order between all components of the plasma compared with the RPA where these effects are neglected.

A more detailed analysis, which accounts for the vertex corrections associated with charge-charge fluctuation, was carried out for an electron gas (EG) in Refs. [56,58,65], where Kukkonen-Overhauser-like effective inter-layer interaction potential [57] were obtained by different approaches. In this scheme we have

$$\hat{W}_{VS}(q,\omega) = \hat{v}_{eff}(q) + \hat{v}_{eff}(q)\hat{\chi}(q,\omega)\hat{v}_{eff}(q) - \hat{U}, \quad (52)$$

with the elements of $\hat{U}$ defined by $v_{ij}(q)G_{ij}(q)$. The form of $W_{12}(q,\omega)$ within the Vignale and Singwi (VS) approach is similar to that in the self-consistent field approach of Singwi *et al*. [55, 54] (SSG) except for the last term. More clearly, the inter-layer interaction in Eq. (52) is given by [58, 65]

$$W_{12}(q,\omega)\,|_{VS} = \frac{v_{12}(q)(1-G_{12}(q))}{\Delta(q,\omega)} - v_{12}(q)G_{12}(q), \quad (53)$$

where

$$\Delta(q,\omega) = [1 - v_{11}(q)(1-G_{11}(q))\chi_1^0(q,\omega,T))\times$$

$$(1 - v_{22}(q)(1-G_{22}(q))\chi_2^0(q,\omega,T)]$$

$$-[v_{12}(q)(1-G_{12}(q)]^2\,\chi_1^0(q,\omega,T)\,\chi_2^0(q,\omega,T).$$

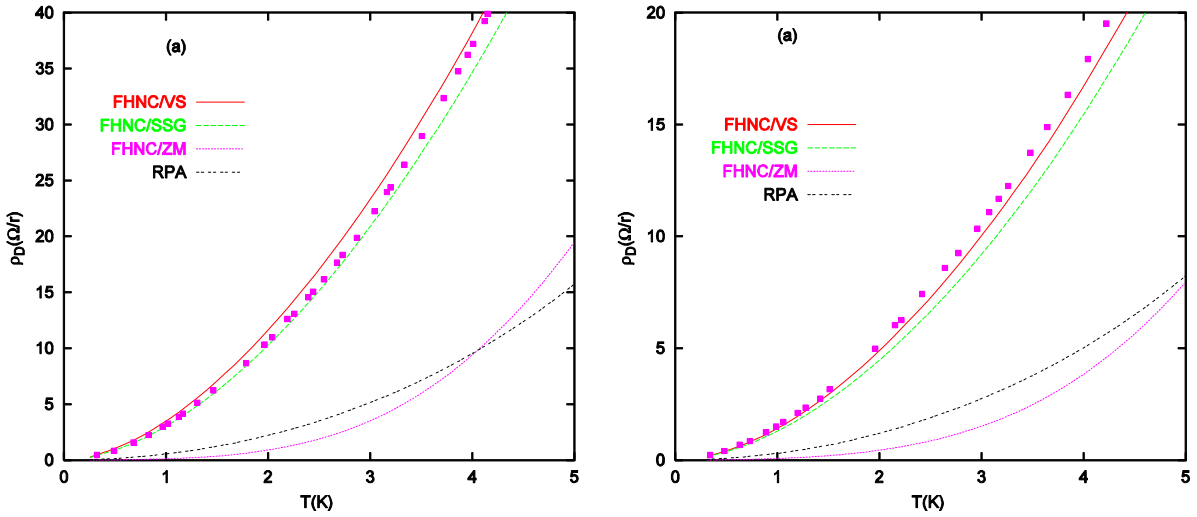

Figure 8. The temperature dependence of the drag resistivity for the identical bilayer electron-electron systems for $n = 3.1\times10^{10}$ cm^{-2} ($r_s = 3.25$) (left panel) and $n = 3.8\times10^{10}$ cm^{-2} ($r_s = 2.93$) (right panel). The full boxes are the experimental data of Ref. [50]. FHNC local-field corrections are used in conjunction with different screened inter-layer interaction models. For more details see Asgari *et al* [67]

Here $\chi_k^0(q,\omega,T)$ is non-interacting charge-charge response function at finite temperature.[48]

Another approximation scheme for screened bilayer 2D electron-electron interaction is proposed by Zheng and MacDonald [66](ZM). In this scheme the screened electron-electron interaction potential is given as

$$\hat{W}_{ZM}(q,\omega) = \left[1 - \hat{\chi}^0(q,\omega,T)\hat{v}_{eff}(q)\right]^{-1}\hat{v}(q). \qquad (55)$$

This is derived essentially from a two-component generalization of the vertex function that enters in self-energy in the so-called $GW\Gamma$ approximation. However, because of the matrix nature of two-component systems there seems to be some ambiguity in such a construction. Note, for instance, that $\hat{W}_{ZM}$ is not a symmetric matrix for unmatched bilayer systems. Finally, we remark that VS, SSG and ZM forms of the effective electron-electron interactions reduce to RPA if the LFCs are omitted.

As it is clear from Eqs. (51), (52) and (55) the local-field corrections are the fundamental quantities for an evaluation of the effective electron-electron interaction. Here, we intend to examine the inter-layer potential of the Coulomb bilayer system by including correlation effects. To this purpose, we made use of the STLS approach both at zero (STLS0) and finite temperature (STLS) schemes. The STLS theory embodies correlations beyond the RPA approach and as an important improvement. In this approach the static LFC that accounts for correlation effects among carriers in the layers k and l are given by:

$$G_{kl}(q) = -\frac{1}{n}\int\frac{dq'}{(2\pi)^2}\frac{q.k}{q^2}\frac{v_{kl}(q')}{v_{kl}(q)}[S_{kl}(|q-q'|)-\delta_{kl}], \quad (56)$$

where $S_{kl}(q)$ is a static structure factor. The equations of motion for the Wigner distribution functions in a bilayer coupled with the linear-response theory yield in the Singwi *et al*[54] approach the following expression for the density-density response functions:

$$\chi_{kl}(q,\omega) = \chi_k^0(q,\omega,T)\times \frac{\left\{\delta_{kl} + (-1)^{\delta_{kl}} v_{kl}(q)(1-G_{kl}(q))\chi_l^0(q,\omega,T)\right\}}{\Delta(q,\omega)}. \quad (57)$$

The fluctuation-dissipation theorem leads to the static structure factor for a bilayer at finite temperature

$$S_{kl}(q) = -\frac{\hbar}{\pi\sqrt{n_k\, n_l}}\int d\omega \Im m\chi_{kl}(q,\omega)\coth\left(\frac{\hbar\omega}{2k_BT}\right). \quad (58)$$

Equations (56), (57) and (58) are solved numerically in a self-consistent way for $G_{kl}(q)$ both at zero and finite temperature cases separately.

Another sophisticated method is based on Fermi hypernetted-chain approach (FHNC). Our strategy follows a similar approach to our recent works, Ref. [38] which uses accurate intra- and inter-layer static structure factors to build the local-field corrections. For this purpose we implement the self consistent Fermi hypernetted-chain approach [10, 11, 12] at zero temperature in order to calculate the intra- and inter-layer static structure factors incorporating the finite thickness effects in a quantum well. The latter effects are known to be important for the adequate description of the drag resistivity from a number of calculations.[52, 55, 48, 59] In what follows we explain the FHNC approximation and then outline our method to obtain the static local-field corrections, $G_{ij}(q)$, at zero temperature.

In Fig. 8 we show the calculated drag resistivity as a function of temperature for various theoretical models of effective inter-layer interaction (i.e. models denoted as

VS, SSG and ZM) with different LFCs (i.e. schemes denoted as FHNC, STLS and STLS0) at layer densities 3.1×10^{10} cm^{-2} and 3.8×10^{10} cm^{-2} and compare them with the experimental results of Kellogg *et al.*[50] The experimental data were obtained for bilayer GaAs-AlGaAs heterostructures for two identical infinite layers of electrons separated by $d = 280$ Å and with a double quantum well of widths $L = 180$ Å. In all our results, the drag resistivity calculated within the VS inter-layer potential is larger than the one calculated within the SSG approximation. It means that the value of U increases with increasing $G_{12}(q)$, and VS potential in Eq. (52) becomes highly different from the SSG potential given by Eq. (51). The static LFCs which are constructed within the FHNC approach together with the electron-electron inter-layer potential calculated within VS and SSG approaches give results in quite good agreement with experimental measurements especially in the low temperature regime below the plasmon-mediated drag.

5. One-dimensional electron liquids

5.1. The Luttinger liquid paradigm

As we move to strongly correlated electron liquids in 1D, it will be useful to briefly recall the main points of Landau's theory of normal Fermi liquids. The basic assumption of Landau's theory is that low-energy excitations are quasiparticles with a very long lifetime and can be treated by means of a simple free-energy functional involving deviations from the Fermi ideal-gas momentum distribution. The theory predicts that the low-temperature thermodynamic properties of an interacting Fermi liquid are very similar to those of the non-interacting system: the interactions only lead to quantitative renormalizations.

A *normal Fermi liquid* is defined as a fluid of interacting fermions whose ground state may be obtained in a continuous manner from that of the ideal gas. In this case:

(a) The Fermi surface still exists as a surface in k space across which the ground-state momentum distribution $n(k)$ has a discontinuity. However, $n(k)$ has a high-momentum tail due to the promotion of some particles outside the Fermi sphere: when the interactions are switched on, the particles correlate their motions and the kinetic energy necessarily increases. The magnitude of the discontinuity in the momentum distribution across the Fermi surface is now less than 1. The increase in kinetic energy is accompanied by a gain in potential energy even in the case of repulsive interactions, with a net gain in the total energy.

(b) The elementary single-particle excitations still are particles and holes, but are well defined only near the Fermi surface.

The properties of the 1D *Luttinger liquids* of interacting fermions are fundamentally different from those of $2D$ or $3D$ normal Fermi liquids [3, 68]. Their elementary excitations are not quasiparticles, but rather collective oscillations of the charge and spin densities, which in general propagate at different speeds giving rise to *spin-charge* separation. Most correlation functions show non-universal power laws with interaction-dependent parameters. Luttinger-liquid behavior is experimentally well established in the physics of quantum Hall edge states and of quantum spin chains. In contrast, it has been argued that presently available quantum wire systems are not in the regime where Luttinger-liquid effects are important [69].

In this Section our main aim is to trace the line of argument that leads to the exactly soluble Tomonaga-Luttinger model [70] (LM) and then to the concept of Luttinger liquid after inclusion of the spin degree of freedom. We thus start by considering a 1D system of non-interacting spinless fermions, with parabolic dispersion $e_k = k^2/(2m)$ ($\hbar = 1$). In its ground state the single-particle states with $|k| < k_F$ are occupied and those with $|k| > k_F$ are empty, k_F being related to the 1D particle density n by $k_F = \pi n$ (in the spinless case). For low-energy excitations (within a momentum cutoff Λ, say) only the region around the two Fermi ``points" at $\pm k_F$ is involved, and in this region (the ``low-energy sector") the dispersion relation can be linearized as $e_{k,\pm} = e_0 \pm v_F k$, with $e_0 = \varepsilon_F - v_F k_F$. In the LM one lets the cutoff Λ go to infinity. There then are two branches of particles, the right movers R (with positive velocity) and the left movers L (with negative velocity). This modification makes the spinless model exactly soluble even when interactions are switched on.

Let $\hat{\rho}_\alpha(q)$ be the Fourier components of the particle density operator,

$$\hat{\rho}_\alpha(q) = \sum_k \hat{c}^\dagger_{\alpha,k+q}\hat{c}_{\alpha,k}\,, \tag{59}$$

for right and left movers, with $\alpha = +$ or $-$ (R or L). The non-interacting Hamiltonian H_0 (and a more general model including interactions, see below) can be written in terms of these operators: in essence, one cannot add a particle (or a hole) to the 1D system without creating at the same time a density wave. A proof of this result is based on the following facts:

(i) the density fluctuation operators obey bosonic commutation relations,

$$[\hat{\rho}_\alpha(-q), \hat{\rho}_{\alpha'}(q')] = \delta_{\alpha\alpha'}\delta_{qq'}\frac{\alpha q L}{2\pi}\,, \tag{60}$$

where L is the system size (special care is needed in calculating the ``anomalous commutator" $[\hat{\rho}_\alpha(-q), \hat{\rho}_\alpha(q)]$);

(ii) $\hat{\rho}_\pm(q)$ creates eigenstates of H_0 with energy $\pm q v_F$, so that H_0 can be rewritten as

$$H_0 = v_F \sum_{q>0,\alpha} \alpha q \hat{\rho}_\alpha(q)\hat{\rho}_\alpha(-q)\,, \tag{61}$$

The linearization of the dispersion relation implies that all electron-hole pairs have the *same energy* qv_F

independently of k, so that the states created by the density fluctuation operator are coherent linear combinations of individual electron-hole excitations;

(iii) the spectra of the fermionic and bosonic representations of H_0 are thus the same (one can demonstrate that the degeneracies of the levels are also the same).

The next step in the development of the spinless LM involves the switching on of the interactions starting from the basic interaction Hamiltonian $H_{int} = \frac{1}{2L}\sum_{q\neq 0} v_q \hat{n}_q \hat{n}_{-q}$ where v_q is the Fourier transform of the interparticle potential and $\hat{n}_q$ is the particle density fluctuation operator. There are two basic types of scattering processes contributing to H_{int}: forward scattering (at $q \approx 0$ in the low-energy sector), and backward scattering (at $q \approx 2k_F$ in the low-energy sector), so that in a conventional notation H_{int} is rewritten as

$$H_{int} = \frac{1}{2L}\sum_{q\neq 0,\alpha} [V_1(q)\hat{\rho}_\alpha(-q)\hat{\rho}_\alpha(q) + V_2(q)\hat{\rho}_{-\alpha}(-q)\hat{\rho}_\alpha(q)]. \quad (62)$$

The couplings are related to the interparticle potential by $V_1(q) = v_q$ and $V_2(q) = v_q - v_{2k_F}$.

The Hamiltonian of the spinless LM in Eqs. (61) and (62), being expressed solely in terms of density fluctuation operators, can be rewritten as

$$H_{LM} = \sum_{q\neq 0}[\left(v_F + \frac{V_1(q)}{2\pi}\right)|q|\hat{b}_q^\dagger \hat{b}_q + \frac{V_2(q)}{4\pi}|q|\left(\hat{b}_q^\dagger \hat{b}_{-q}^\dagger + \hat{b}_{-q}\hat{b}_q\right)] \quad (63)$$

where

$$\hat{b}_q = \sqrt{\frac{2\pi}{L|q|}}[\Theta(q)\hat{\rho}_R(q) + \Theta(-q)\hat{\rho}_L(q)] \quad (64)$$

The Hamiltonian (63) can be diagonalized by a Bogoliubov transformation, with the result

$$H_{LM} = \sum_{q\neq 0}\omega_q \hat{\beta}_q^\dagger \hat{\beta}_q, \quad (65)$$

where $\omega_q = c_q|q|$ with

$$c_q = \sqrt{\left[v_F + \frac{V_1(q)}{2\pi}\right]^2 - \left[\frac{V_2(q)}{2\pi}\right]^2}. \quad (66)$$

The boson operators are linear combinations of the original density fluctuation operators, so that the elementary excitations of the Hamiltonian (65) are coherent superpositions of collective density oscillations. Evidently, the stability condition

$$|2\pi v_F + V_1(q)| > |V_2(q)|, \quad (67)$$

must be satisfied for the dispersion relation to be real. In addition, the ground-state wave function is normalizable if the stability condition

$$\lim_{q\to\infty}\frac{q^{1/2}V_2(q)}{2\pi v_F + V_1(q)} = 0, \quad (68)$$

is satisfied. Notice that in the non-interacting gas limit one recovers zero sound in the Fermi gas ($\omega_q = v_F|q|$): the electron-hole pairs have been replaced by this collective excitation.

In the case of short-range interactions the dispersion relation (66) describes sound waves at long wavelengths, when the coupling parameters tend to constant values ($V_1(q) \to 2g_4$ and $V_2(q) \to g_2$, say). One can prove that in this limit the Hamiltonian (65) can be transformed into a continuum-model Hamiltonian describing an elastic string:

$$H_{LM} = \frac{1}{2}\int dx\left[\pi u K \Pi^2(x) + \frac{u}{\pi K}[\partial_x \phi(x)]^2\right]. \quad (69)$$

Here the fields $\phi(x)$ and $\Pi(x)$, obeying canonical commutation relations $[\phi(x), \Pi(x')] = i\delta(x-x')$, are related to the particle density $\rho(x)$ and to the current density $J(x)$ by $\partial_x\phi(x) = -\pi[\rho(x) - \rho_0]$ and $J(x) = uK\Pi(x)$, ρ_0 being the average particle density in the ground state. The parameters in Eq. (69) are

$$\begin{cases} u = \sqrt{\left(v_F + \frac{g_4}{\pi}\right)^2 - \left(\frac{g_2}{2\pi}\right)^2}, \\ K = \sqrt{\frac{2\pi v_F + 2g_4 - g_2}{2\pi v_F + 2g_4 + g_2}}. \end{cases} \quad (70)$$

The form of the transformed Hamiltonian in Eq. (69) emphasizes the collective nature of the particle motions on a chain: a particle setting out with a given momentum will collide with a first neighbor and exchange momentum with it to start a density wave along the chain.

We merely quote without proof at this point two remarkable properties of the quantum fluid described by the LM:

(a) *Momentum distribution*. The momentum occupation number $n_{k,\alpha}$ has the same form for right and left movers and obeys the relation

$$n_{k_F+\delta k,\alpha} = 1 - n_{k_F-\delta k,\alpha}. \quad (71)$$

Thus $n_{k_F,\alpha} = 1/2$ (as in the Fermi gas), but the function $n_{k,\alpha}$ is continuous through k_F. However, for any non-vanishing interaction the momentum distribution and the density of states have power-law singularities at the Fermi level, with a vanishing single-particle density of states at E_F. The absence of a step discontinuity at k_F implies the absence of a quasiparticle pole in the one-particle Green's function.

(b) *Electrical conductance*. The current I flowing through a homogeneous 1D fluid subject to a potential drop ΔV applied between a source (at the left) and a drain (at the right) is the difference between the current carried by right movers driven by the source potential towards the drain and the current of left movers driven by the drain potential towards the source. The value of I is determined by the proper current-density – charge-

density response function, and in the spinless LM this function coincides with that of the non-interacting fluid. The result is $I = G\Delta V$ where the conductance G has the fundamental value

$$G = e^2 / h \tag{72}$$

(or twice this value if spin is included).

5.2. Model with spin-1/2 and spin-charge separation

Up to this point we have ignored the spin of the electron. Upon inclusion of the spin-$1/2$ degree of freedom, all operators in Eqs. (61) and (62) acquire a spin index σ and summations over σ need adding. However, $2k_F$-scattering of pairs of electrons with antiparallel spins can now also be accompanied by spin flips, and inclusion of this effect makes the model no longer exactly soluble in general. If this term is neglected, one gets the Luttinger-liquid Hamiltonian in the form

$$\begin{aligned} H_{LL} &= v_F \sum_{q>0,\alpha,\sigma} \alpha q \hat{\rho}_{\alpha,\sigma}(q)\hat{\rho}_{\alpha,\sigma}(-q) \\ &+ \frac{1}{2L}\sum_{q\neq 0} V_1(q)[\,\hat{\rho}_R(q)+\hat{\rho}_L(q)][\,\hat{\rho}_R(-q)+\hat{\rho}_L(-q)] \\ &+ \frac{1}{2L}\sum_{q\neq 0,\sigma}[V_2(q)-V_1(q)]\times \\ &[\,\hat{\rho}_{R,\sigma}(-q)\hat{\rho}_{L,\sigma}(q)+\hat{\rho}_{L,\sigma}(-q)\hat{\rho}_{R,\sigma}(q)], \end{aligned} \tag{73}$$

where $\hat{\rho}_\alpha = \sum_\sigma \hat{\rho}_{\alpha,\sigma}$. One can now carry out a transformation to boson operators, using Eq. (64) with spin-indexed operators, and eliminate the cross terms between charge and spin density by introducing spin-symmetric and spin-antisymmetric combinations,

$$\begin{cases} \hat{b}_q^C = \frac{1}{\sqrt{2}}\left(\hat{b}_{q\uparrow} + \hat{b}_{q\downarrow}\right), \\ \hat{b}_q^S = \frac{1}{\sqrt{2}}\left(\hat{b}_{q\uparrow} - \hat{b}_{q\downarrow}\right), \end{cases} \tag{74}$$

with the result $H_{LL} = H_C + H_S$ where

$$\begin{aligned} H_C &= \sum_{q\neq 0}\{\left[v_F + \frac{V_1(q)}{\pi}\right]|q|\hat{b}_q^{C\dagger}\hat{b}_q^C + \\ &\frac{V_1(q)+V_2(q)}{4\pi}|q|\left(\hat{b}_q^{C\dagger}\hat{b}_{-q}^{C\dagger} + \hat{b}_{-q}^C\hat{b}_q^C\right)\}, \end{aligned} \tag{75}$$

$$\begin{aligned} H_S &= \sum_{q\neq 0}[v_F|q|\hat{b}_q^{S\dagger}\hat{b}_q^S + \\ &\frac{V_2(q)-V_1(q)}{4\pi}|q|\left(\hat{b}_q^{S\dagger}\hat{b}_{-q}^{S\dagger} + \hat{b}_{-q}^S\hat{b}_q^S\right)]. \end{aligned} \tag{76}$$

Each of these two independent terms can be diagonalized by a Bogoliubov transformation, finding two branches of excitations: charge density waves propagating with velocity

$$c_q^C = \sqrt{\left[v_F + \frac{V_1(q)}{\pi}\right]^2 - \left[\frac{V_1(q)+V_2(q)}{2\pi}\right]^2}, \tag{77}$$

and spin density waves propagating with velocity

$$c_q^S = \sqrt{v_F^2 - \left[\frac{V_2(q)-V_1(q)}{2\pi}\right]^2}, \tag{78}$$

Spin-charge separation is implicit in the fact that these two velocities are in general different. Thus, if we write the spin-indexed boson operator as the sum of a charge component and a spin component by inversion of Eq. (74), these two components will evolve in time according to two different and independent Hamiltonians, and will propagate at different velocities.

The last term in the Hamiltonian (73) includes only $2k_F$-scattering between parallel-spin electrons. Adding a spin-flip back-scattering term in the form

$$\begin{aligned} H_{sf} = \frac{g_1}{L}\sum_{k,p,q}\sum_{\sigma,\sigma'}&\hat{c}_{R,\sigma}^\dagger(k)\hat{c}_{L,\sigma'}^\dagger(p)\hat{c}_{R,\sigma'}(p+2k_F+q)\times \\ &\hat{c}_{L,\sigma}(k-2k_F-q), \end{aligned}$$

then the Hamiltonian can be written as

$$H = H_C + H_S + \frac{2g_1}{(2\pi A)^2}\int dx\cos(\sqrt{8}\phi_S(x)), \tag{80}$$

where for $i = \mathrm{C,S}$ we have

$$H_i = \frac{1}{2}\int dx\left[\pi u_i K_i \Pi_i^2(x) + \frac{u_i}{\pi K_i}[\partial_x\phi_i(x)]^2\right] \tag{81}$$

with

$$\begin{cases} u_i = \sqrt{\left(v_F + \frac{g_{4,i}}{\pi}\right)^2 - \left(\frac{g_i}{2\pi}\right)^2}, \\ K_i = \sqrt{\frac{2\pi v_F + 2g_{4,i} - g_i}{2\pi v_F + 2g_{4,i} + g_i}}. \end{cases} \tag{82}$$

(see Eqs. (69) and (70)), having defined $g_C = g_1 - 2g_2$, $g_S = g_1$, $g_{4,C} = g_4$, and $g_{4,S} = 0$. For $g_1 = 0$ Eqs. (79)-(81) describe independent long-wavelength oscillations of the charge and spin density with linear dispersion relations $\omega_i = u_i|q|$. For $g_1 \neq 0$ the last term on the RHS of Eq. (80) must be treated perturbatively by means of a renormalization-group approach, and the results are as follows.

(i) *Repulsive interactions*. For $g_1 > 0$ the cosine term in Eq. (80) is renormalized to zero at long wavelengths, so that spin-flip processes become irrelevant in the renormalization-group sense. A similar fate is met by corrections to the Hamiltonian (80) such as those associated with band curvature and with the absence of high-energy single-particle states. Lattice effects intervene at low energy only to give rise to higher harmonics at wave numbers of the form $q = (2n+1)k_F$ where n is an integer.

(ii) *Attractive interactions*. In the case $g_1 < 0$, however, the renormalization group scales to strong coupling. In this case the elementary excitations of the spin-fluctuation field ϕ_S may, for instance, correspond to small oscillations around one of the minima of the cosine term, or possibly to soliton-like terms where ϕ_S goes from one minimum to the other. Both types of spin excitation have a finite activation energy: thus for $g_1 < 0$ the spin excitation spectrum has a gap, whereas

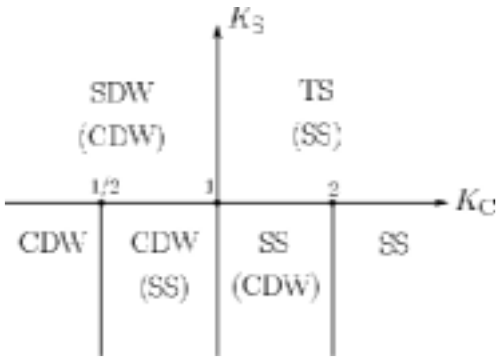

Figure 9. Phase diagram of the 1D system of spin-$1/2$ fermions. The spin sector is massless in the upper part ($K_S > 1$), while in the lower part ($K_S < 1$) the spin excitations are massive (*i.e.* with gap).

the charge excitation spectrum remains ``massless'' (*i.e.* gapless).

Figure 9 reports the phase diagram for the 1D system of spin-$1/2$ fermions for isotropic spin couplings as assumed so far, in the (K_C, K_S) plane. The plane is divided into four sectors depending on the value of the parameter K_C and of the back-scattering g_1 (or equivalently of the parameter K_S, with the two upper sectors corresponding to $g_1 > 0$ and the two lower sectors to $g_1 < 0$). The indicated phases correspond to the most divergent susceptibility, while the subdominant divergences are indicated in parentheses. The symbols CDW and SDW indicate charge-density-wave and spin-density-wave phases (see Fig. 9). Also present are singlet superconductivity (SS) and triplet superconductivity (TS).

5.3. Impurity in Luttinger liquids

Let us now consider the effect of a single *impurity* on the density of the Luttinger liquid. For simplicity we assume that the electron-impurity potential is a δ-function of dimensionless strength u located at $x = 0$, *i.e.* $V_{e-i}(x) = \mathrm{h} v_F u \delta(x)$. The electron density operator in real space is given by

$$\hat{n}(x) \approx \hat{n}_0(x) + \hat{n}_{2k_F}(x), \tag{83}$$

where

$$\hat{n}_0(x) = \hat{\psi}_R^\dagger(x)\hat{\psi}_R(x) + \hat{\psi}_L^\dagger(x)\hat{\psi}_L(x) \tag{84}$$

is the part associated with zero-momentum transfer (*i.e.* forward scattering) and

$$\hat{n}_{2k_F}(x) = \hat{\psi}_R^\dagger(x)\hat{\psi}_L(x) + \hat{\psi}_L^\dagger(x)\hat{\psi}_R(x) \tag{85}$$

is the part associated with momentum transfer $\pm 2k_F$ (*i.e.* back-scattering). The electron impurity interaction term operator is thus

$$\hat{V}_{e-i} = \mathrm{h} v_F u \left[\hat{n}_0(0) + \hat{n}_{2k_F}(0) \right] \tag{86}$$

It is intuitively clear that the forward scattering term simply multiplies the one-electron wave functions by a position-dependent phase factor, with no observable consequences. On the other hand, the back - scattering

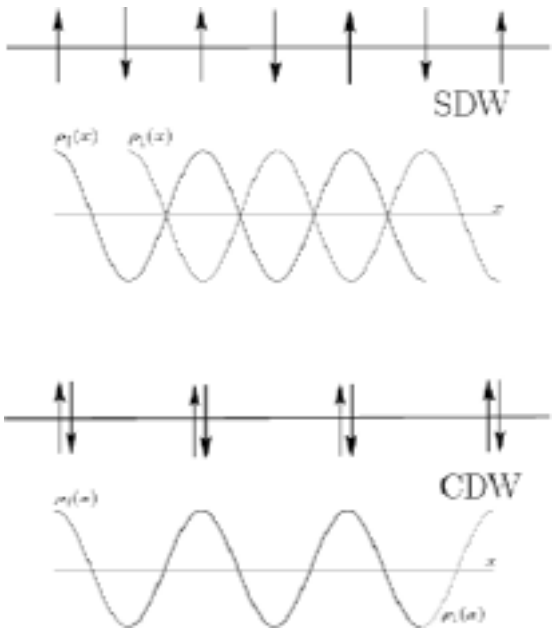

Figure 10. Schematic drawing of a spin-density wave (SDW) and a charge-density wave (CDW) with wavelength $2\pi/(2k_F)$. In a SDW one has two waves of spin density for up and down spins, with wavelength $2\pi/(2k_F)$: the two waves are shifted relative to each other by half a wavelength and form antiferromagnetic ordering. In a CDW the two waves are in phase giving a charge-density modulation and no spin-density modulation.

term has important and unexpected consequences:

(a) *Friedel oscillations and charge density waves.* The Friedel oscillations of the displaced electron density around a charged impurity in a normal 1D electron fluid have the form $\cos(2k_F x)/|x|$, where the wavelength $2\pi/(2k_F)$ is equal to the mean first-neighbor distance L/N in the spinless case. The role of repulsive interactions in the LM is to multiply the above factor by a function expressing an extremely slow spatial decay. Of course, any form of long-range order such as Wigner crystallization is prevented by fluctuations in 1D according to the Wagner-Mermin theorem. One may rather view the spinless LM fluid as being prone to formation of a charge-density modulation having wave number $2k_F$ and slowly decaying amplitude, with the role of the impurity being that of pinning the phase of such a modulation. Inclusion of the spin-$1/2$ degree of freedom adds to the above result for the screening charge a term having the form $\cos(4k_F x)$ multiplied again by an extremely slow decay factor. Predisposition to charge density waves with wavelength $2\pi/(4k_F) = L/N$ (with k_F being now equal to $\pi n/2$) is indicated in the repulsive Luttinger liquid.

(b) *Back-scattering current.* Inclusion of a point-like impurity in the fluid causes a back-scattering current, which is due to the transfer of right movers across the wire to the left-moving branch minus the transfer of left movers to the right-moving branch. The result is a reduction of the net current flowing through the wire at a given value of ΔV. The conductance of the channel is

reduced accordingly to

$$G = \frac{e^2}{h} - \frac{d I_B}{d(\Delta V)}, \qquad (87)$$

The back-scattering current I_B is proportional to $(\Delta V)^{2g-1}$, where (i) $g = 1$ in the absence of interactions, so that ohmic behavior is preserved though with a reduced conductance; but (ii) $g < 1$ for repulsive interactions, implying a vanishing conductance for $\Delta V \to 0$. Pinning of the electron density by the impurity is again indicated.

5.4. Long-range interactions and Wigner crystallization

Up to here we have assumed that the electron-electron interaction is of finite range, *i.e.* the $q \to 0$ limit of $V_1(q)$ and $V_2(q)$ is finite. This is not unreasonable in many situations, since the one-dimensional system is usually embedded within a larger three-dimensional structure which eventually screens the coulomb interaction at sufficiently large distance. It is of interest, however, to see what happens in the ideal case of the bare coulomb interaction. The long wavelength limit of bare 1 *D* coulomb interaction has the form $2e^2 \mid \ln(qb) \mid$, b being the wire radius, hence we recover from Eq. (66) a plasma-like dispersion relation,

$$\omega_q = C \mid q \parallel \ln(qb) \mid^{1/2}, \qquad (88)$$

where the constant $C = \sqrt{2v_F e^2 / \pi \mathrm{h}(1 + v_{2k_F} / 2\pi \mathrm{h} v_F)}$, reduces to the RPA [75] value: $\sqrt{2ne^2 / m}$, if $v_{2k_F} = 0$. Allowing for a finite value of v_{2k_F} may be said to introduce an effective mass correction.

The most interesting point here is the extremely slow decay (much slower than any power low) of the $4k_F$ component, showing an incipient CDWs at wavevector $4k_F$. This oscillation period is exactly the average interparticle spacing, *i.e.* the structure is that expected for a one dimensional Wigner crystal. Again, because of the one dimensional nature of the model, there is no true long range order, however, the extremely slow decay of the $4k_F$ oscillation would produce strong quasi Bragg peaks in a scattering experiment. It is worthwhile to point out that this $4k_F$ contribution arises even if the coulomb interaction is extremely weak and depends only on the long range character of the interaction. On the other hand, correlation functions that involve operators changing the total number of particles (*e.g.* the single particle Green's function and pairing correlation functions) decay faster than any power low: $\exp[-c \ln^{-3/2}(x)]$, c being a constant. This in particular means that the momentum distribution function n_k and all its derivatives are continuous at k_F, and there is only an essential singularity at this point.

Many of the electron-electron interaction effects become increasingly important as carrier density and dimensionality are reduced and the homogenous electron liquid provides a primitive model for their study. The crucial role in the theory is played by the particle pair distribution function $g(z)$. In our previous works we presented a theory of the pair distribution function and other ground-state properties of the 3D and 2D electron liquid [16 , 30]. The theory was based on a Fermi hypernetted-chain approximation (FHNC) which represents a direct generalization to the Fermi systems of the well known hypernetted-chain Euler-Lagrange (HNC/EL) approximation. One of the important feature of theory based on HNC/EL or FHNC is that the theory sums not only all ring and ladder diagrams exactly, but also mixed diagrams in a local approximation [72]. It means the FHNC theory is not a Fermi liquid theory and therefore we able to apply it for studying many-body effects on 1D EL. As we shall see, much higher sophistication is needed to attain a quantitatively useful theory in 1D EL. We shall have to dwell on terms beyond the FHNC/0, which includes elementary diagrams and the three-body Jastrow-Feenberg correlations. These effects have been studied theoretically in boson fluids for the 1D system using the HNC/EL formalism by Krotscheck *et al* [17].

We consider a 1D EL as a model for a system of electronic carriers with band mass m in a semiconductor heterostructure with dielectric constant ε. The resulting effective 1D potential is readily shown [74] to be $v(z) = (e^2 / \varepsilon)(\sqrt{2} / 2b)\, exp[z^2 / 4b^2]\, erfc[|z| / 2b]$ with Fourier transform $v(k) = (e^2 / \varepsilon)\, n\, exp[b^2 k^2]\, E_1[b^2 k^2]$ where the exponential integral function, $E_1(x)$ is defined as $\int_x^\infty e^{-u} du / u$. The Fourier transform is defined according to the general expression $FT[F(r)] = n \int dr F(r) \exp(ik \cdot r)$. Here n is the total average density. The above form of the bare potential exhibits the typical 1D behavior, $v(k) \approx ln(kb)$ as $k \to 0$, and the 3D behavior, $v(k) \approx 1/(kb)^2$ as $k \to \infty$.

We assume that only one subband is occupied and neglect any contribution from higher subbands. This approximation leads to $r_s > \pi b / 4$.

With the zero of energy taken at the chemical potential, the formally exact Euler-Lagrange equation for the spin summed pair distribution function $g(z)$ reads [10, 14]

$$\left[-\frac{\mathrm{h}^2}{m} \frac{d^2}{dz^2} + v(z) + v_B(z) + v_F(z) \right] \sqrt{g(z)} = 0. \qquad (89)$$

Here, $v(z)$ is the 1D EL potential and the Bose-like potential $v_B(z)$ contains the effects of correlations and by itself would determine $g(z)$ in a Bose fluid. The details of the Bose-like potential have been discussed by many authors, for instance see Ref. [12]. We can write it as

$$v_B(z) = w_{ind}(z) + \Delta v_{ele}(z), \tag{90}$$

from the theoretical point of view it is important to remark that in FHNC-type calculations at strong coupling the Bose-like $v_B(q)$ interactions should be corrected by the addition of three-body correlations and elementary-diagrams (or "bridge functions") contributions [10, 11, 18, 12]. The $\Delta v_{ele}(z)$ is a term arising from elementary diagrams and triplet correlations. We only consider the fourth-order elementary diagrams and triplet correlations, $\Delta v_{ele}(k) = w_B^{E_4}(k) + w_B^{(3)}(k)$, which hereafter, we call it as FHNC/4+triplet acronym. Note that the approach is reduced to the Fermi hypernetted-chain approximation, FHNC/0 when the corrections of the Bose-like interaction are omitted, $\Delta v_{ele}(k) = 0$. The contribution from the low-order elementary diagrams to the effective Bose potential is

$$w_B^{E_4}(k) = -\frac{\hbar^2}{4mn}\{\frac{k^2}{2\pi}\varepsilon_4(k) + \int\frac{dq}{(2\pi)}q^2[S(q)-1]\frac{\delta\varepsilon_4(q)}{\delta S(k)}\}, \tag{91}$$

where $\varepsilon_4(q)$ is given by a twofold integral (in 1D) over momentum space.

$$\varepsilon_4(q) = \frac{1}{2n^4}\int\frac{dpdq'}{(2\pi)^2}[S(p)-1]\times [S(q')-1][S(p+q')-1]\times [S(p+q)-1][S(p+q'+q)-1], \tag{92}$$

and the contribution of three-body correlations is given by the integral,

$$w_B^{(3)}(k) = \frac{1}{8n\pi}\int dqS(p)S(q)u_3(q,p,k)\times \{v(q,p,k) + [\varepsilon(p)+\varepsilon(q)]u_3(q,p,k)\} \tag{93}$$

where $p = -(q+k)$, $\varepsilon(k) = \hbar^2k^2/[2mS(k)]$ and, with the definition $X(k) = 1 - S^{-1}(k)$, we have $v(q,p,k) = (\hbar^2/m)[kpX(p) + kqX(q) + pqX(p)X(q)]$ and

$$u_3(q,p,k) = -(\hbar^2/2m)\times \frac{[kpX(p)X(k) + pqX(p)X(q) + kqX(q)X(k)]}{\varepsilon(k)+\varepsilon(p)+\varepsilon(q)}. \tag{94}$$

With regard to the Fermi term $v_F(z)$ in Eq. (88), we adopt the same criteria in determining its form as in Ref. [14]. An important requirement is that Eq. (88) should give the exact fermion distribution function when one goes to the weak-coupling limit $r_s \to 0$, where in this limit $g(z)$ becomes the Hartree-Fock pair distribution function, $g^{HF}(z)$. The Fermi term in the scattering potential is then determined by the Hartree-Fock structure factor $S^{HF}(k)$,

$$v_F(k) = \frac{\hbar^2}{m}FT\left[\frac{d^2\sqrt{g^{HF}(z)}/dz^2}{\sqrt{g^{HF}(z)}}\right] + \frac{\hbar^2k^2}{4m}\left[\frac{S^{HF}(k)-1}{S^{HF}(k)}\right]^2[2S^{HF}(k)+1] - \Delta v_{ele}(k)|_{S(k)=S^{HF}(k)}. \tag{95}$$

The Hartree-Fock static structure function is given by $S^{HF}(k) = (k/k_F)\theta(2k_F - k) + \theta(k - 2k_F)$ where θ is the Heaviside step function, $k_F = \pi/4r_sa_B^*$ is the Fermi wave vector and $g^{HF}(z)$ is given by

$$g^{HF}(z) = 1 - \frac{sin^2(k_Fz)}{2(k_Fz)^2}. \tag{96}$$

The rational behind Eq. (95), is as in Ref. [kallio], (i) the first term on the RHS ensures that the Hartree-Fock limit is correctly embodied into the theory, (ii) the second and third terms ensure that the Bose-like scattering potential is suppressed for electrons at weak coupling [16]. We introduce at this point the relation between $g(z)$ and $S(k)$:

$$g(z) = 1 + \frac{2}{n}\int cos(kz)[S(k)-1]dk. \tag{97}$$

Our numerical results of the pair distribution function of the 1D EL is compared with the DMC data of Ref. [71] in Figure 11. The quantum wire width is $b = 0.1a_B^*$ and the system is highly correlated. We have clearly achieved good qualitatively agreement with the DMC data. It is obvious from the Fig. 11, FHNC/4+triplet results are in excellent agreement with DMC data up to $zk_F < 1.3$ and less agreement in larger z-values to produce the oscillation behavior. The strong oscillation behavior in DMC data corresponds to the periodicity of the quasi-Wigner crystal. It is apparent from the figure that FHNC/4+triplet approach which includes further corrections than FHNC/0, modifies the results and show the first peak and its oscillatory behavior, however the magnitude of peak is less than the one predicted by DMC simulation. Our $g(z)$ has more structure within FHNC/4+triplet than the $g(z)$ obtained within FHNC/0. Moreover, in both approaches the short-range behavior of $g(z)$ give correct shape in base on Kimball's cusp condition and they have different values at contact.

In Figure 12, we show our results for $S(k)$ in the paramagnetic 1D EL at $r_s = 1$ and 2 within both FHNC/0 and FHNC/4+triplet approximations. It is obvious to see the improvements brought above by the use of FHNC/4+triplet over FHNC/0. Apart from the strong peak structure at $q = 4k_F$ which appears in DMC simulation, the FHNC/4+triplet results are in good

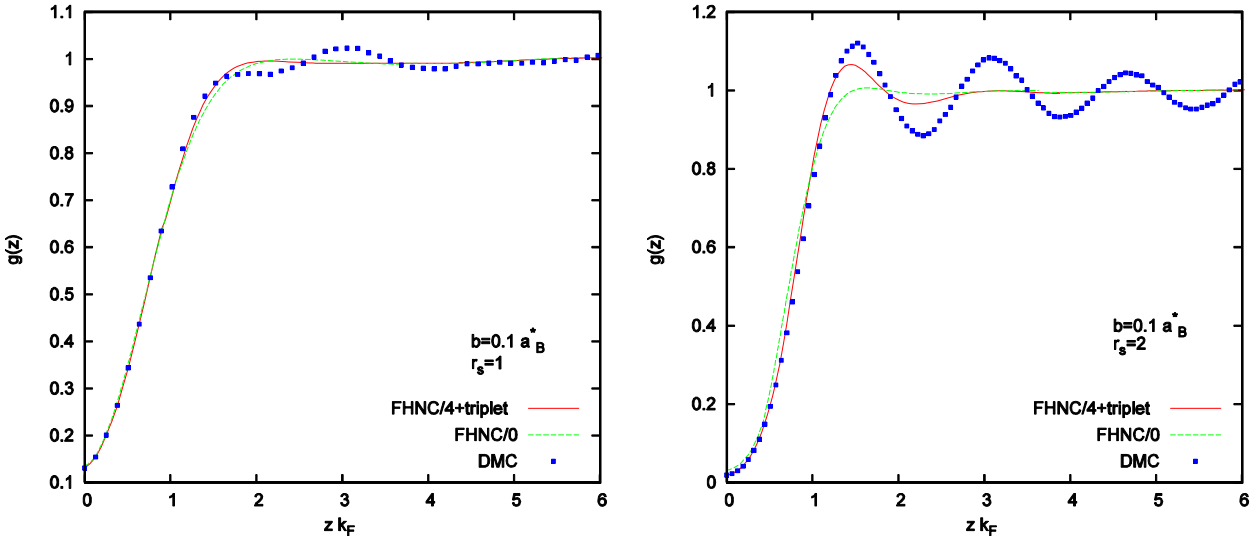

Figure 11. The pair distribution function $g(z)$ as a function of zk_F for various $r_s = 1$, (left panel) and $r_s = 2$ (right panel) at $b = 0.1a_B^*$ comparing the FHNC/0 and FHNC /4 + triplet approximations with DMC data of Casula *et al* [71]. For more details see Asgari [73]

Table 1. Correlation energy of the 1D EL in Ryd/electron. DMC from Casula, [71] STLS from Calmels and Gold [75].

r_s	Various calculations	$b = a_B^*$	$b = 2a_B^*$
0.1	DMC	-0.000463	-0.000110
	Ref.[73]	-0.000459	-0.000107
	STLS	-0.000457	-0.000117
0.2	DMC	-0.0016996	-0.000418
	Ref.[73]	-0.001665	-0.000411
	STLS	-0.001645	-0.000431
0.4	DMC	-0.00579	-0.001514
	Ref.[73]	-0.00564	-0.001502
	STLS	-0.005449	-0.001492
0.6	DMC	-0.01122	-0.003089
	Ref.[73]	-0.01099	-0.002983
	STLS	-0.01044	-0.002955
0.8	DMC	-0.01738	-0.00498
	Ref.[73]	-0.01678	-0.00476
	STLS	-0.01608	-0.00469
1.0	DMC	-0.02394	-0.00709
	Ref.[73]	-0.02296	-0.00687
	STLS	-0.02202	-0.00662
2.0	DMC	-0.05840	-0.01912
	Ref.[73]	-0.05311	-0.01806
	STLS	-0.04968	-0.01735
3.0	DMC	-0.0856	-0.0322
	Ref.[73]	-0.07330	-0.02952
	STLS	-0.06862	-0.02744
4.0	DMC	-0.09986	-0.04372
	Ref.[73]	-0.08518	-0.03814
	STLS	-0.07978	-0.03556

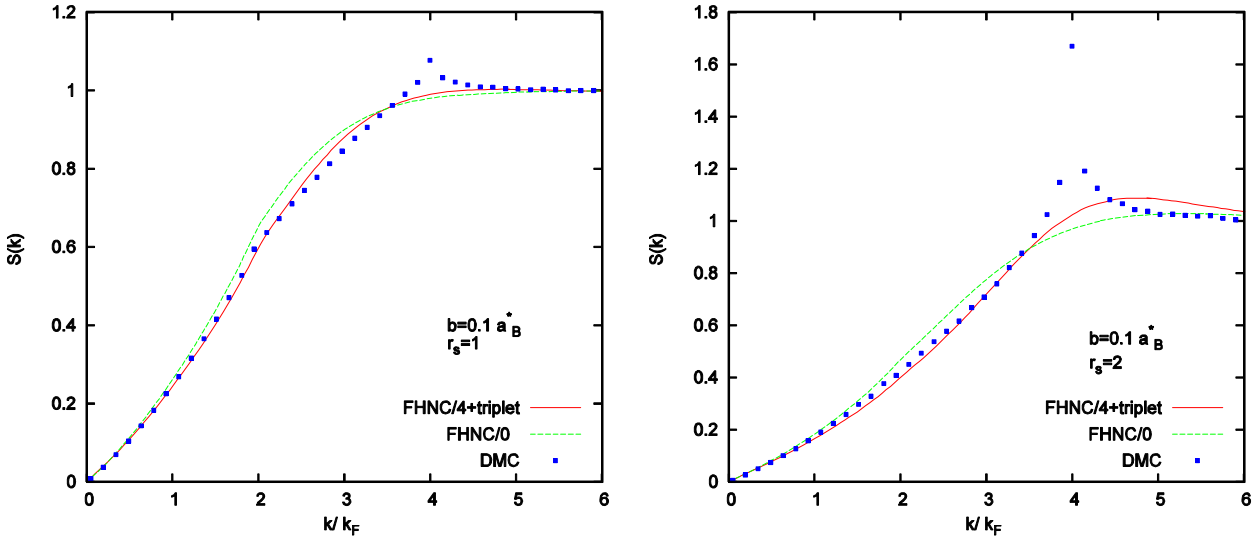

Figure 12. (Color online) The static structure function $S(k)$ as a function of k/k_F for $r_s = 1$ (top panel), $r_s = 2$ (bottom panel) and $b = 0.1a_B^*$ comparing both FHNC/0 and FHNC/4+triplet approximations with DMC data of Casula *et al* [71]. For more details see Asgari [73]

agreement with the DMC data of Casula *et al* [71]. The strong peak has been related to a quasi-order of the electrons [71]. Note that there is no true long-range order in 1D system. We find that as the density is reduced the correlation effects become stronger and $S(k)$ starts to develop a broad peak around $q = 4.5k_F$. The FHNC/0 does not show any peak as the density decreases. Theory gives the correct behavior of the long-wavelength limit of $S(k)$ and the results coincide with the DMC data.

There are several noteworthy points based on the results shown in Figs. 1 and 2. (i) Despite that FHNC gives very good results for the pair distribution function and static structure factor in high dimensional electron liquids [16, 30, 10, 11], it can give qualitative results for 1D EL where the system is highly correlated. (ii) The approach could not produce a strong peak for static structure factor at $q = 4k_F$ which is related to the slow decay of the $4k_F$ components of the charge density-density correlation function.

we present a theoretical study of the pair distribution function, the effective electron-electron interaction and the correlation energy of the 1D electron liquid where the system is strongly correlated. Our approach yields numerical results of good agreement in comparison with recent diffusion Monte Carlo studies[71]. We showed that the long-wavelength behavior of the static structure factor is in agreement with the bosonization findings for the Coulomb Luttinger liquid. The charge excitation spectrum is calculated and it is expected to give better results when compared to experimental measurements in intermediate r_s values and even large momentum limit where the Random Phase approximation calculation is no longer accurate. Moreover, the small k behavior of the charge excitation spectrum is shown be equivalent with the bosonization findings. Improvements of the theory will be necessary for a quantitative study of the physical quantities and the correlation energy. As we have mentioned in the main text, we only considered the low-order elementary diagrams and the three-body corrections in the theory is based on Fermi hypernetted-chain approximation. We believe inclusion of the contributions of the fifth-order and higher elementary diagrams will improve our results. Moreover as we mentioned in the main text, we used a practical recipe of FHNC approach [10] by replacing Jastrow product factor to the square of the Slater determinant describing the non-interacting fermions gas wave-functions. This recipe of FHNC reduces correlation respect to the full FHNC-EL theory. Although it is little affect in high dimensions but it may be important in the specific case of a 1D EL.

6. Conclusion

In this review article, I started an introductory information of the theory of many-body systems and then discussed a number of recent developments in the understanding of electron liquids. After an introductory section aiming to convey the spirit of many-body physics by reference to long-standing problems and ideas. To this purpose I give our recent theory dealing with microscopic properties of many-body physics and show the results in based on the extended version of FHNC. Our theory is free from any fitting parameters. To justify how the theory is, we compare some physical quantities with those calculated within available the state-of-the-art Quantum Monte Carlo in different distensibilities in the highly strongly correlated regions. Furthermore, we calculate the quasiparticle properties for strictly or quasi 2D EL and compare our microscopic calculations with those measured by recent experimental groups. Moreover, we carry out numerical results for a bilayer electron system and for an application, we comparative study the charge Coulomb drag effect in bilayer electron

system incorporating the electron-electron interactions and the characteristic of samples. We compare our transresistivity calculated with those measured by experiments. In all cases our results were in very good agreement with relate quantity calculated within Quantum Monte Carlo or available experimental data in correlated systems. I would like to thanks Dr Akbarzadeh, Dr Shahbazi and Dr Jafari for organizing the summer school on Strongly correlated systems, took place in Isfehan, on June 2007.

References

1. G F Giuliani and G Vignale, *Quantum Theory of the Electron Liquid* Cambridge University Press, Cambridge, England (2005).
2. S Giorgini, L P Pitaevskii and S Stringari, arXiv:0706.3360.
3. T Giamarchi, *Quantum Physics in One Dimension* Clarendon Press, Oxford (2004).
4. D R Hartree, *Proc. Cambridge Phil. Soc*. **24** (1928) 89 and 111; V Fock, Zs. Phys. **61** (1929) 126; J C Slater, *Phys. Rev*. **35** (1930) 210.
5. S Abedinpour, *PhD Thesis, SNS*, Pisa, Italy (2007).
6. N W Ashcroft ang N D Mermin, *Solid Sate Physics*, by Hort and Wiston (1976).
7. R E Peierls, *Quantum Theory of Solids,* Clarendon Press, Oxford (1955).
8. R M Dreizler and E K U Gross, *Density Functional Theory, An Approach to the Quantum Many-Body Problem* Springer Berlin (1990).
9. B Davoudi, M Polini, R Asgari and M P Tosi, *Phys. Rev*. B **66** (2002) 075110; B Davoudi, R Asgari, M Polini and M P Tosi, Phys. Rev. B **67** (2003) 172503; F Capurro, R Asgari, B Davoudi, M Polini, and M P Tosi, *Z. Naturforsch*. **57a** (2002) 237.
10. L J Lantto and P J Siemens, *Nuclear Phys*. A **317** (1979) 55; L J Lantto, *Phys. Rev*. B **36** (1987) 5160.
11. J G Zabolitzky, *Phys. Rev*. B **22** (1980) 2353.
12. For a recent review see E Krotscheck and M Saarela, *Phys. Rep*. **232** (1993) 1.
13. T Chakraborty, *Phys. Rev*. B **25** 3177 and **26** (1982) 6131; T. Chakraborty. A. Kallio, L. J. Lantto, and P. Pietiläinen, Phys. Rev. B **27** (1983) 3061.
14. A Kallio and J Piilo, *Phys. Rev. Lett*. **77** (1996) 4237.
15. G Ortiz, M Harris and P Ballone, *Phys. Rev. Lett*. **82** (1999) 5317.
16. B Davoudi, R Asgari, M Polini, M P Tosi, *Phys. Rev*. B **68** (2003) 155112.
17. E Krotscheck, M Saarela, *Phys. Rep.* **232** (1993) 1.
18. V Apaja, J Halinen, V Halonen, E Krotscheck, M Saarela, *Phys. Rev*. B **55** (1997) 12925.
19. R A Smith, A Kallio, M Puoskari, P Toropainen, *Nucl. Phys*. A **328** (1979) 186.
20. S De Palo, S Conti, S Moroni, *Phys. Rev*. B **69**, (2004) 035109.
21. P Gori-Giorgi, S Moroni, G B Bachelet, *Phys. Rev*. B (2004).
22. C Attaccalite, S Moroni, P Gori-Giorgi, and G B Bachelet, *Phys. Rev. Lett*. **88**, (2002) 256601.
23. R Asgari, B Davoudi, M P Tosi, *Solid State Commun.* **131**, (2004) 301.
24. L D Landau, Sov. Phys. JEPT, **3** (1957) 920.
25. I K Marmorkos and S Das Sarma, *Phys. Rev*. B **44** R3451 (1991); J D Lee and B I Min, *Phys. Rev*. B **53,** 10 (1996) 988; H-J Schulze, P Schuck, and N Van Giai, *Phys. Rev.* B **61** (2000) 8026.
26. S Yarlagadda and G F Giuliani, *Phys. Rev*. B **49** (1994) 7887; **61** (2000) 12556; C S Ting, T K Lee, and J J Quinn, *Phys. Rev. Lett*. **34** (1975) 870.
27. H M Böhm and K Schörkhuber, *J. Phys.: Condens. Matter* **12** (2000) 2007.
28. Y Zhang and S Das Sarma, *Phys. Rev*. B **71** (2005) 045322; S Das Sarma, V M Galitski, and Y Zhang, *Phys. Rev*. B **69** (2004) 125334.
29. Y Zhang, V M Yakovenko, and S Das Sarma, *Phys. Rev*. B **71** (2005) 115105.
30. R Asgari, B Davoudi, M Polini, G F Giuliani, M P Tosi, and G Vignale, *Phys. Rev*. B **71** (2005) 045323.
31. R Asgari, B Davoudi and B Tanatar, *Solid State Commun*. **130** (2004) 13.
32. V T Dolgopolov, *JETP Lett*. **76** (2002) 377.
33. B Spivak, *Phys. Rev.* B **64** (2001) 085317.
34. Y-W Tan, J Zhu, H L Stormer, L N Pfeiffer, K W Baldwin, and K W West *Phys. Rev. Lett*. **94** (2005) 016405.
35. S De Palo, M Botti, S Moroni, and G Senatore *Phys. Rev. Lett*. **94** (2005) 226405.
36. B Davoudi, M Polini, G Giuliani, M P Tosi, *Phys. Rev*. B **64** (2001) 153101.
37. C A Kukkonen and A W Overhauser, *Phys. Rev*. B **20** (1979) 550.
38. R Asgari, A L Suba s , A A Sabouri-Dodaran, and B Tanatar, *Phys. Rev*. B **74** (2006) 155319.
39. J Zhu, H L Stormer, L N Pfeiffer, K W Baldwin, and K W West, *Phys. Rev. Lett*. **90** (2003) 056805; Y-W Tan, J Zhu, H L Stormer, L N Pfeiffer, K W Baldwin, and K W West, *Phys. Rev*. B **73** (2006) 045334.
40. R Asgari and B Tanata, *Phys. Rev*. B **74** (2006) 075301.
41. T M Rice, *Solid State Phys*. **32** (1977) 1; J C Hensel, T G Phillips, and G A Thomas, *ibid.* **32** (1977) 88.
42. L V Keldish and Y V Kopaev, *Fiz, Tverd, Tela, Leningard* **6** (1964) 2791; *Sov. Phys. Solid State* **6** (1965) 2219; A N Kozolov and L A Maximov, *Zh. Eksp. Teor. Fiz*. **48** (1965) 1184; *Sov. Phys. JETP* **21** (1965) 790; L V Keldish and A N Kozlov, *Zh Eksp. Teor. Fiz*. **54** (1968) 1978; *Sov. Phys. JETP* **27** (1968) 521.
43. Yu E Lozovik and V I Yudson, *Pis`ma Zh. Eksp. Teor. Fiz*. **22** (1975) 556; *JETP Lett*. **22** (1975) 274; *Sold state Commun*. **19** (1976) 391; *Zh. Eksp. Teor. Fiz.* **71** (1976) 738; *Sov. Phys. JETP* **44** (1976) 389.
44. S De Palo, F Rapisarda and G Senatore, *Phys. Rev*.

Lett. **88** (2002) 206401.
45. S Abedpour, R Asgari, M Polini and M P Tosi, *Solid State Commun*. **144** (2007) 65.
46. A Punnoose and A M Finkelstein, *Science* **310** (2005) 289.
47. N P R. Hill, J T Nicholls, E H Linfield, M Pepper, D A Ritchie, G A C Jones, B Y-K Hu and K Flensberg, *Phys. Rev. Lett*. **78** (1997) 2204.
48. K Flensberg and B Y-K Hu, *Phys. Rev*. B **52** (1995) 14796.
49. H Noh, S Zelakiewicz, X G Feng, T J Gramila, L N Pfeiffer, and K W West, *Phys. Rev*. B **58** (1999) 12621.
50. M Kellogg, J P Eisenstein, L N Pfeiffer, and K W West, *Solid State Commun*. **123** (2002) 515.
51. R Pillarisetty, H Noh, D C Tsui, E P De Poortere, E Tutuc, and M Shayegan, *Phys. Rev. Lett*. **89** (2002) 016805.
52. A P Jauho and H Smith, *Phys. Rev*. B **47** (1993) 4420.
53. L Zheng and A H MacDonald, *Phys. Rev*. B **48** (1993) 8203.
54. K S Singwi, M P Tosi, R H Land, and A Sjölander, *Phys. Rev*. **176** (1968) 589.
55. L S′wierkovski, J Szyman s′ki, Z W Gortel, *Phys. Rev. Lett*. **74** (1995) 3245; *Phys. Rev*. B **55** (1997) 2280.
56. A Yurtsever, V Moldoveanu and B Tanatar, *Solid State Commun*. **125** (2003) 575.
57. C A Kukkonen and A W Overhauser, *Phys. Rev*. B **20** (1979) 550.
58. G Vignale and K S Singwi, *Phys. Rev*. B **31** (1985) 2729.
59. S M Badalyan, C S Kim, G Vignale and G Senatore, *Phys. Rev*. B **75** (2007) 125321.
60. S De Palo, F Rapisarda and G Senatore, *Phys. Rev. Lett*. **88** (2002) 206401 and references therein.
61. G Vignale and A H MacDonald, *Phys. Rev. Lett*. **76** (1996) 2786; B Y-K Hu, *Phys. Rev. Lett.* **85** (2000) 820.
62. D S Kainth, D Richards, H P Hughes, M Y Simmons and D A Ritchie, *J. Phys.: Condens. Matter* **12** (2000) 439.
63. A Kamenev and Y Oreg, *Phys. Rev*. B **52** (1995) 7516.
64. B Y-K Hu, *Aust J. Phys*. **53** (2000) 107.
65. C F Richardson and N W Aschroft, *Phys. Rev*. B **52** (1997) 15 130.
66. L Zheng and A H MacDonald, *Phys. Rev*. B **49** (1994) 5522.
67. R Asgari, B Tanata and B Davoudi, *Phys. Rev*. B, **77** (2008) 115301.
68. J Voit, *Rep. Progr. Phys*. **58** (1995) 977; H J Schulz, G Cuniberti and P Pieri, *in Field Theories for Low-Dimensional Condensed Matter Systems*, edited by G Morandi, P Sodano, A Tagliacozzo, and V Tognetti Springer, Berlin (2000).
69. D W Wang, A J Millis, and S Das Sarma, *Phys. Rev. Lett*. **85** (2000) 4570.
70. S Tomonaga, *Progr. Theor. Phys*. **5** (1950) 544; J M Luttinger, *J. Math. Phys.* **4** (1963) 1154; D C Mattis and E H Lieb, ibid. **6** (1965) 304; A Luther and I Peschel, *Phys. Rev*. B **9** (1974) 2911; F D M Haldane, *J. Phys*. C **14** (1981) 2585.
71. Michele Casula and Gaetano Senatore, *Chem. Phys. Chem* **6** (2005) 1902; Michele Casula, Sandro Sorella and Gaetano Senatore, *Phys. Rev*. B **74** (2006) 245427.
72. A D Jackson, A Lande and R A Smith, *Phys. Rev. Lett*. **54** (1986) 1469; E Krotscheck, R A Smith and A D Jackson, *Phys. Rev*. A **33** (1986) 3535; A Lande and R A Smith, *Phys. Rev*. A **45** (1992) 913.
73. R Asgari, *Solid State Commuin*. **141** (2007) 563.
74. W I Friesen and B Bergersen, *J. Phys*. C **13** (1980) 6627.
75. L Calmels and A Gold, *Phys. Rev*. B **56** (1997) 1762.
76. A W Overhauser, Can. *J. Phys*. **73** (1995) 683; P. Gori-Giorgi and J. P. Perdew, *Phys. Rev*. B **64** (2001) 155102.